Electronic Supplementary Information for

Multidimensional H-atom Tunneling in Catecholate Monoanion

Debabrata Bhattacharyya and Sai G. Ramesh

Department of Inorganic and Physical Chemistry, Indian Institute of Science, C. V. Raman Road, Bangalore 560012, India

Contents

I. Ab initio potential

Fig. S1 shows the 2D ab initio potential in the TS normal mode space. In each Q_1-Q_x potential plot, all other coordinates are fixed at 0 (their TS value). The corresponding plot with the DGEVB$^+$ potential is given in Fig. 5 of the manuscript. Overlaid on the contours are the full-dimensional IRC path projected onto these 2D subspaces. Along the transfer mode, that these paths terminate far from the 2D minimum $|Q_1|$ is expected as the EQM value of $|Q_1|$ is approximately twice as large. Note, however, that the IRC end point *values* of Q_7, Q_{13}, and Q_{27} are close to their 2D minimum positions, indicating their weak coupling to the transfer mode and overall lower energetic importance. Contrariwise, the IRC end points of Q_5, Q_{10} and Q_{29} are further away. These deviations indicate again the modes' importance as well as the multidimensional nature of the tunneling.

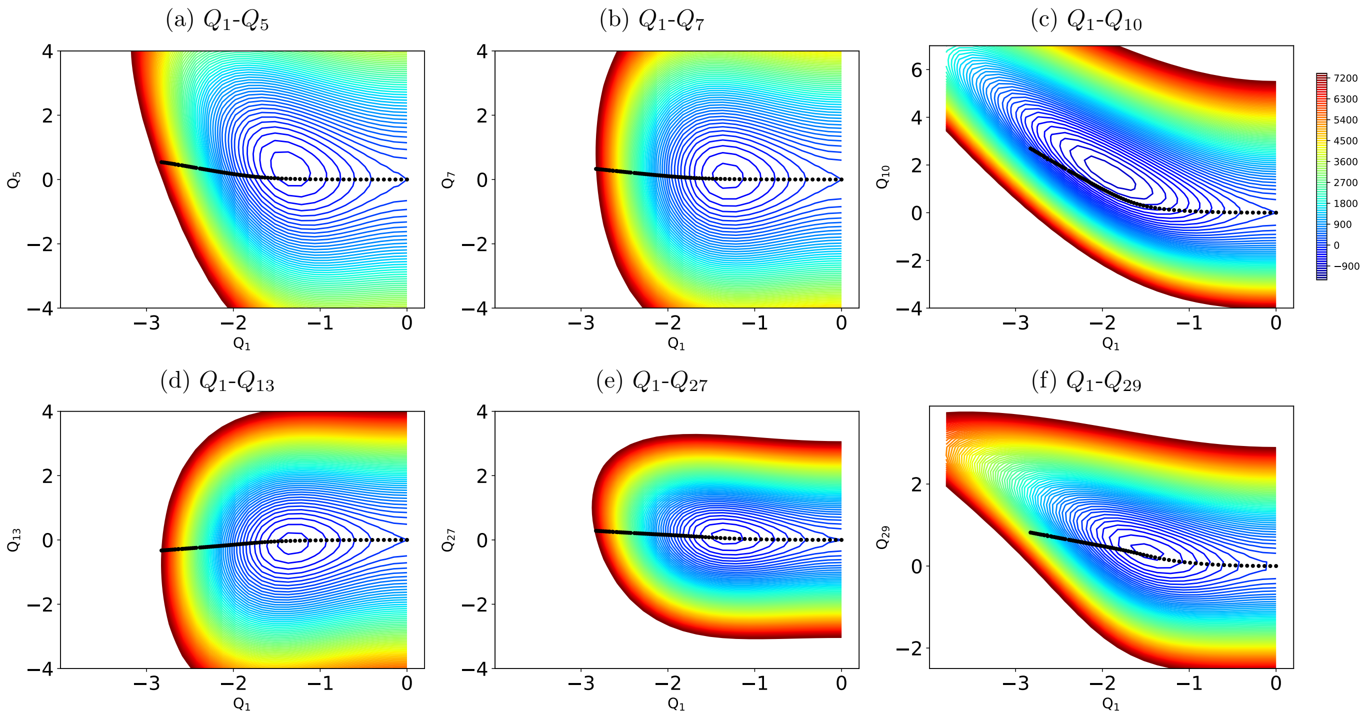

FIG. S1. **Two-dimensional contours of the ab initio potential.** The contour spacing is 100 cm^{-1}. A common contour colour bar is provided on the top right that indicates the energy range covered.

II. Sudden vector projection

The sudden vector projection method[1] gives the projection of each equilibrium mode on the imaginary frequency mode at the TS. Larger projections indicate the importance of the corresponding equilibrium mode to tunneling. Most

TABLE S1. **Sudden vector projection** of each EQM mode on to Q_1.

Mode	Sym	$\lvert k_{1j}\rvert$	Mode	Sym	$\lvert k_{1j}\rvert$	Mode	Sym	$\lvert k_{1j}\rvert$	Mode	Sym	$\lvert k_{1j}\rvert$
$\mathcal{Q}_1$	A''	0.0000	$\mathcal{Q}_{10}$	A''	0.0000	$\mathcal{Q}_{18}$	A'	0.1078	$\mathcal{Q}_{26}$	A'	0.0540
$\mathcal{Q}_2$	A''	0.0000	$\mathcal{Q}_{11}$	A'	0.0320	$\mathcal{Q}_{19}$	A'	0.0036	$\mathcal{Q}_{27}$	A'	0.0879
$\mathcal{Q}_3$	A'	0.6123	$\mathcal{Q}_{12}$	A''	0.0000	$\mathcal{Q}_{20}$	A'	0.2333	$\mathcal{Q}_{28}$	A'	0.2430
$\mathcal{Q}_4$	A''	0.0000	$\mathcal{Q}_{13}$	A''	0.0000	$\mathcal{Q}_{21}$	A'	0.0027	$\mathcal{Q}_{29}$	A'	0.0118
$\mathcal{Q}_5$	A'	0.0381	$\mathcal{Q}_{14}$	A''	0.0000	$\mathcal{Q}_{22}$	A'	0.3274	$\mathcal{Q}_{30}$	A'	0.0109
$\mathcal{Q}_6$	A''	0.0000	$\mathcal{Q}_{15}$	A''	0.0000	$\mathcal{Q}_{23}$	A'	0.2020	$\mathcal{Q}_{31}$	A'	0.0079
$\mathcal{Q}_7$	A'	0.0235	$\mathcal{Q}_{16}$	A'	0.0445	$\mathcal{Q}_{24}$	A'	0.1169	$\mathcal{Q}_{32}$	A'	0.0013
$\mathcal{Q}_8$	A'	0.0044	$\mathcal{Q}_{17}$	A'	0.0350	$\mathcal{Q}_{25}$	A'	0.2273	$\mathcal{Q}_{33}$	A'	0.4328
$\mathcal{Q}_9$	A''	0.0000									

recently in the work on tropolone by Houston et al.,[2] it was used to succesfully predict the set of equilibrium modes that can enhance tunneling. In the present case, it is computed as $|k_{1j}|$ from the expression $Q_1 = Q_1(\boldsymbol{x}_{eqm}) + k_{1j}\mathscr{Q}_j$; see also Eq. 3 of Wang and Bowman.[3] Its values given below in Table S1 point to modes $\mathscr{Q}_3$, $\mathscr{Q}_{33}$ and the set of modes $\mathscr{Q}_{20} - \mathscr{Q}_{28}$ as those that promote tunneling. In TS mode terms, these map (Section 2.2.2 of the manuscript) to Q_1, Q_{10}, and Q_{29}, which are key modes for the tunneling process in catecholate monoanion.

III. Eigenstates with unrelaxed potentials

The multidimensional nature of the H-atom tunneling was shown in Section 2.1 of the manuscript through both the significant sizes of displacements along seven modes – Q_1, Q_5, Q_7, Q_{10}, Q_{13}, Q_{27}, and Q_{29} – and also the observation that a very large fraction of the full barrier height is recovered when only these modes move from their EQM to TS positions. Here, we explore the structure of eigenstates in various $n = 2$, 3 and 4 mode spaces with unrelaxed potentials (i.e. all other modes are fixed to zero.)

For various such S_{nu} mode spaces, the eigenstates were obtained via the PODVR approach; see Section 3.1 of the manuscript. In particular Table 5 of the manuscript gives the number of PODVR functions used for various coordinates (in parentheses in the last column). In 2D, however, the direct product size with primitives is small enough to make a direct comparison of eigenvalues obtained with them and with the corresponding PODVR direct product basis. In doing so, e.g. for the 2D Q_1-Q_{10}, Q_1-Q_5, and Q_1-Q_{29} eigenstates, we found the energy difference to be less than 1 cm^{-1} for most states with energy less than 5000 cm^{-1}. With these encouraging results, we have used PODVRs for 3D and 4D calculations. Note that the basis sizes shown in parentheses in the Table 5 are the final sizes that were taken for multidimensional calculations. The convergence of all multidimensional calculations were checked with slightly lower basis sizes after the states were characterized; these are also given in several tables below.

A. 2D eigenstates

Several past works have analysed the role of coupling strength, frequency and symmetry in multidimensional tunneling using simple model potentials.[4–8] For catecholate monoanion, we present below the eigenstates in various $S_{2u} = (Q_1, Q_x)$ spaces with unrelaxed potentials. The characterisation of the eigenstates reveals the role of Q_x in enhancing or suppressing tunneling upon mode-specific vibrational excitation. We emphasize that the focus is not on tunneling splitting magnitudes for the anion (which cannot be compared to any experiments from these 2D results) but rather just their trends with identifiable excitations/assignments. The present results should be treated as the first step to higher dimensional eigenstates in unrelaxed mode-spaces discussed in later sections in this ESI as well as the manuscript (7D).

1. Q_1-Q_{10} Eigenstates

The CO scissor Q_{10} is strongly coupled to Q_1. The effective minimum of the DGEVB$^+$ potential in this 2D space is about -960 cm^{-1} (the full minimum is about -1568 cm^{-1}). The first few eigenstates in Q_1-Q_{10} subspace are given in Table S2 while their plots are given in Fig. S2. The convergence of these states is given in Table S3.

The descriptions in the table immediately indicate the mixed nature of most of the listed states. The lowest two are the ground tunneling pair $\nu_{gs}^{\pm}$ eigenstates; see Figs. S2a and b. The ground state tunneling splitting is about 241 cm^{-1}. This large value is owing to the reduced barrier compared to the full dimensional case; as the number of dimensions is increased the ground state tunneling splitting does decrease systematically.

The description for state $M = 3$ (of even parity) is still dominated by the $1_{0^+}10_0$, while that of $M = 4$ (of odd parity) is mostly of $1_{0^-}10_1$ character. However, plots c and d in Fig. S2 for these states show that there is one node along Q_{10} for both with no node and one node along Q_1, respectively. This supports the labels ν_{10}^{+} and ν_{10}^{-} for them. Similarly, nodal patterns for plots of state pairs (5, 6), (7, 9) and (10, 11) allow their assignment as $n\nu_{10}^{\pm}$, $n = 2-4$. However, this identification is not easily seen from the state descriptions. This may be attributed to the strong coupling between the two modes.

We finally note that the (8, 14) pair in Table S2 sees the dominance of the $1_{1^\pm}10_0$ in the description, prompting their assignment as $\nu_1^{\pm}$. These are supported by their plots in parts k and l of Fig. S2; their nodal pattern clearly show eigenstates with one quantum of excitation along Q_1.

We now turn to the pattern of tunneling splittings. The increase from the $\nu_{gs}^{\pm}$ pair to the $\nu_1^{\pm}$ pair is the expected trend along the tunneling coordinate Q_1. With increasing Q_{10} excitation, the tunneling splitting also increases significantly, i.e. it promotes tunneling. Recall that Q_{10} is the CO symmetric scissor (A_1) motion which brings the two oxygen atoms closer. Excitations in this mode bring about increased probability density on the concave side of the IRC path. This region has been recognised to have the tunneling path in the literature for the large curvature tunneling cases involving symmetrically coupled modes.[9,10]

TABLE S2. **Two-dimensional eigenstates in Q_1-Q_{10} subspace, their description, assignment, and tunneling splittings.** They are listed in tunneling split pairs as seen from the labels including ($\pm$) parity. M is a serial index. Each state eigenvalue E_M (relative to the TS energy) and excitation energy E_M^{ex} (relative to $M = 1$) are given, along with a description in terms of direct products of 1D eigenbases. Only those direct products with a contribution (squared coefficient) of 5% or more are listed. The tunneling splitting value Δ is given for each identified pair. All energies are in cm^{-1}.

M	Label	E_M	E_M^{ex}	Δ	Description
1	v_{gs}^{+}	192.1	0.0		$+0.7111\ 1_{0^+}10_0$ $+0.3949\ 1_{0^+}10_1$ $+0.2847\ 1_{1^+}10_1$ $+0.2702\ 1_{0^+}10_2$ $+0.2265\ 1_{1^+}10_2$
2	v_{gs}^{-}	434.0	241.9	241.9	$+0.9318\ 1_{0^-}10_0$
3	v_{10}^{+}	617.6	425.5		$+0.6632\ 1_{0^+}10_0$ $-0.3432\ 1_{0^+}10_1$ $-0.2710\ 1_{0^+}10_2$ $-0.2674\ 1_{1^+}10_2$ $+0.2646\ 1_{0^+}10_3$ $+0.2484\ 1_{1^+}10_3$
4	v_{10}^{-}	921.4	729.3	303.8	$+0.8160\ 1_{0^-}10_1$ $-0.3097\ 1_{0^-}10_0$ $+0.2483\ 1_{1^-}10_2$ $+0.2304\ 1_{0^-}10_2$
5	$2v_{10}^{+}$	1071.7	879.6		$+0.6981\ 1_{0^+}10_1$ $+0.2623\ 1_{1^+}10_0$ $+0.2360\ 1_{0^+}10_4$ $+0.2355\ 1_{1^+}10_4$ $+0.2337\ 1_{1^+}10_3$
6	$2v_{10}^{-}$	1422.1	1230.0	350.4	$+0.7171\ 1_{0^-}10_2$ $-0.3868\ 1_{0^-}10_1$ $-0.2863\ 1_{1^-}10_3$ $-0.2343\ 1_{0^-}10_4$ $+0.2316\ 1_{1^-}10_1$ $-0.2269\ 1_{0^-}10_3$
7	$3v_{10}^{+}$	1552.3	1360.2		$+0.6237\ 1_{0^+}10_2$ $+0.3430\ 1_{1^+}10_1$ $-0.2377\ 1_{1^+}10_6$ $-0.2284\ 1_{0^+}10_1$ $+0.2263\ 1_{1^+}10_5$
9	$3v_{10}^{-}$	1946.9	1754.8	394.6	$+0.6327\ 1_{0^-}10_3$ $+0.4334\ 1_{0^-}10_2$ $+0.3061\ 1_{1^-}10_4$ $+0.2545\ 1_{0^-}10_5$ $-0.2338\ 1_{1^-}10_2$
10	$4v_{10}^{+}$	2039.9	1847.8		$+0.5587\ 1_{0^+}10_3$ $-0.3674\ 1_{1^+}10_2$ $+0.2999\ 1_{0^+}10_2$ $+0.2375\ 1_{1^+}10_7$
11	$4v_{10}^{-}$	2473.1	2281.0	433.2	$+0.5647\ 1_{0^-}10_4$ $-0.4446\ 1_{0^-}10_3$ $+0.3179\ 1_{1^-}10_5$ $-0.2680\ 1_{0^-}10_6$
8	v_1^{+}	1818.4	1626.3		$+0.7782\ 1_{1^+}10_0$ $-0.3092\ 1_{0^+}10_2$ $-0.3086\ 1_{0^+}10_1$ $+0.2844\ 1_{1^+}10_1$
14	v_1^{-}	2790.3	2598.2	971.9	$+0.9358\ 1_{1^-}10_0$ $-0.2637\ 1_{0^-}10_1$

TABLE S3. **Convergence of Q_1-Q_{10} states.** The energy eigenvalues E_M, where M is a serial index, are given with respect to the TS energy as the reference zero of energy. The state labels follow the corresponding eigenstate table in the manuscript. The tunneling splittings between identified state pairs (arranged successively in the table) is Δ. All energies and tunneling splittings are in cm^{-1}. In parenthesis in table header is number of PODVR basis functions, N_α^{PO}, for each coordinate, α. (See also Table 5 of the manuscript.) The final column indicates the fractional percentage change in tunneling splitting between the highest and penultimate basis used. For all convergence checks, the $N_1^{PO} = 18$ was held fixed as its highest 1D eigenvalues surpassed 50000 cm^{-1} for that size.

M	Label	E_M		Δ		$\lvert\%\Delta_{err}\rvert$
		(18, 17)	(18, 15)	(18, 17)	(18, 15)	
1	v_{gs}^{+}	192.12	192.21			
2	v_{gs}^{-}	433.95	433.95	241.83	241.74	0.04
3	v_{10}^{+}	617.57	617.86			
4	v_{10}^{-}	921.42	921.48	303.85	303.62	0.08
5	$2v_{10}^{+}$	1071.66	1069.95			
6	$2v_{10}^{-}$	1422.12	1422.22	350.46	352.27	0.52
7	$3v_{10}^{+}$	1552.30	1547.28			
9	$3v_{10}^{-}$	1946.87	1945.86	394.57	398.58	1.02
10	$4v_{10}^{+}$	2039.91	2038.13			
11	$4v_{10}^{-}$	2473.05	2468.88	433.14	430.75	0.55
8	v_1^{+}	1818.41	1818.28			
14	v_1^{-}	2790.30	2790.28	971.89	972.0	0.01

TABLE S4. **Two-dimensional eigenstates in Q_1-Q_{29} subspace.** The columns follow the description given in Table S2.

M	Label	E_M	E_M^{ex}	Δ	Description
1	v_{gs}^{+}	953.5	0.0		$+0.8146\ 1_{0^+}29_0$ $+0.5548\ 1_{1^+}29_0$
2	v_{gs}^{-}	1392.9	439.4	439.4	$+0.9193\ 1_{0^-}29_0$ $+0.3664\ 1_{1^-}29_0$
3	v_1^{+}	2307.7	1354.2		$+0.6589\ 1_{1^+}29_0$ $-0.5082\ 1_{0^+}29_0$ $+0.4421\ 1_{0^+}29_1$ $+0.2523\ 1_{2^+}29_0$
4	v_1^{-}	3015.4	2061.9	707.7	$+0.7328\ 1_{0^-}29_1$ $+0.5892\ 1_{1^-}29_0$
5	v_{29}^{+}	3174.4	2220.9		$+0.6471\ 1_{0^+}29_1$ $+0.5354\ 1_{1^+}29_1$ $-0.3943\ 1_{1^+}29_0$ $-0.2282\ 1_{2^+}29_0$
7	v_{29}^{-}	4050.3	3096.8	875.9	$+0.6132\ 1_{1^-}29_0$ $-0.5139\ 1_{1^-}29_1$ $-0.5039\ 1_{0^-}29_1$ $-0.2240\ 1_{0^-}29_0$
6	$2v_1^{+}$	3904.1	2950.6		$+0.5735\ 1_{1^+}29_1$ $+0.5035\ 1_{2^+}29_0$ $-0.4432\ 1_{0^+}29_1$ $+0.3470\ 1_{0^+}29_2$
8	$2v_1^{-}$	4667.3	3713.8	763.2	$+0.6012\ 1_{0^-}29_2$ $+0.5332\ 1_{1^-}29_1$ $-0.4035\ 1_{2^-}29_0$ $-0.2566\ 1_{0^-}29_1$

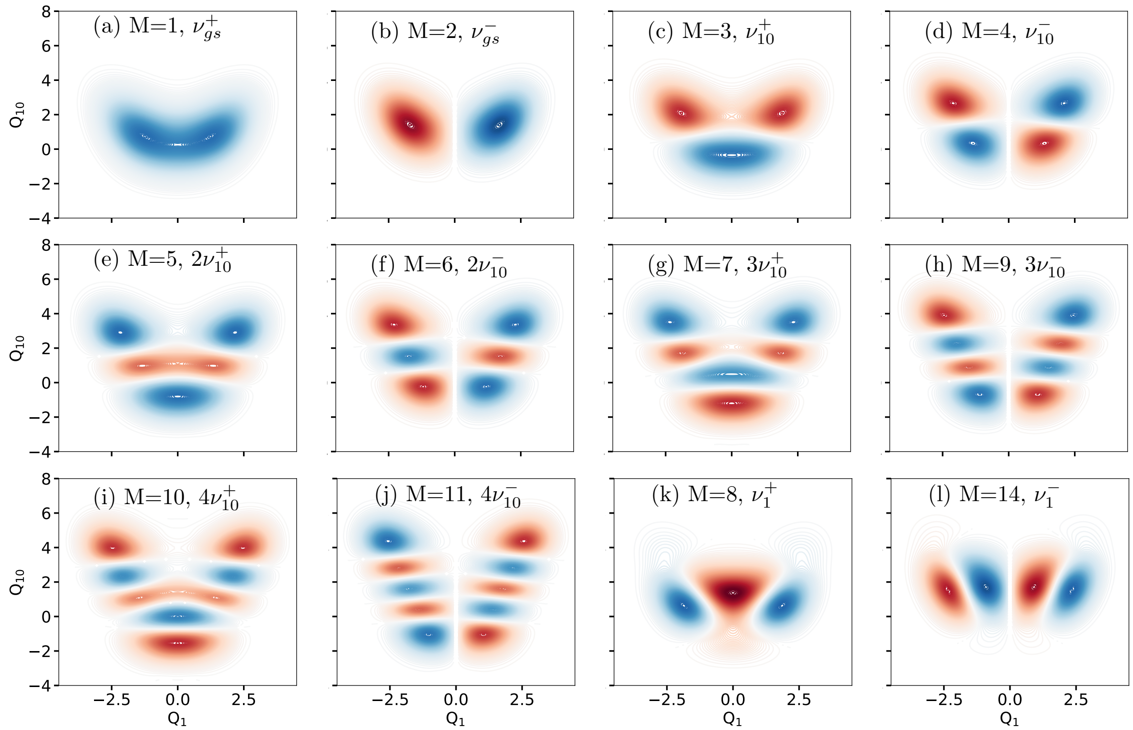

FIG. S2. **Plots of Q_1-Q_{10} eigenstates.** The descriptions of these states are given in Table S2. The labelling is consistent with the nodal pattern in each plot.

TABLE S5. **Convergence of Q_1-Q_{29} states.** The states listed match those given in the corresponding table of the manuscript. See the caption of Table S3 for notational details.

M	Label	E_M		Δ		$\|\%\Delta_{err}\|$
		(18, 7)	(18, 6)	(18, 7)	(18, 6)	
1	ν_{gs}^{+}	953.46	949.30			
2	ν_{gs}^{-}	1392.90	1392.14	439.44	442.84	0.77
3	ν_{1}^{+}	2307.68	2293.10			
4	ν_{1}^{-}	3015.43	2996.49	707.75	703.39	0.62
5	ν_{29}^{+}	3174.37	3169.29			
7	ν_{29}^{-}	4050.30	4045.74	875.93	876.45	0.06
6	$2\nu_{1}^{+}$	3904.14	3899.12			
8	$2\nu_{1}^{-}$	4667.30	4654.82	763.16	755.70	0.98

2. Q_1-Q_{29} *Eigenstates*

Q_{29} is the second most important mode after Q_{10}. This also is symmetrically coupled to Q_1, although less coupled compared to Q_{10}. The effective barrier height in the Q_1-Q_{29} space is about 642 cm^{-1}. The first eight states are listed in Table S4, the last of which which surpasses $\sim$5000 cm^{-1} from the 2D minimum. The convergence of the states is given in Table S5. Along Q_{29}, we have investigated states up to one quanta of excitation as it has a high local frequency. Contour plots of the eigenstates are given in Fig. S3. Assignment of states and labeling notation has been done in the same fashion as for the Q_1-Q_{10} case.

It is evident from Table S4 that eigenstate assignment in the Q_1-Q_{29} space is more complex than that for Q_1-Q_{10} due to smaller differences in leading coefficients. Here, too, most states are difficult to be assigned to a single direct product state. The figures of the eigenstates also show different nodal patterns than those for Q_1-Q_{10} eigenstates; we remark that the nodes themselves are locally perpendicular to very curved wavefunctions.

The lowest two states are $\nu_{gs}^{\pm}$. The states $M = 3$ and 4, labelled as $\nu_1^{\pm}$, have one quantum of excitation in Q_1 with even and odd parity, respectively. This assignment is done mainly based on nodal structure. Similarly, states $M = 6$ and 8 are assigned as $2\nu_1^{\pm}$, while $M = 5$ and 7 are assigned as $\nu_{29}^{\pm}$. From Table S4, it is evident that these pairs

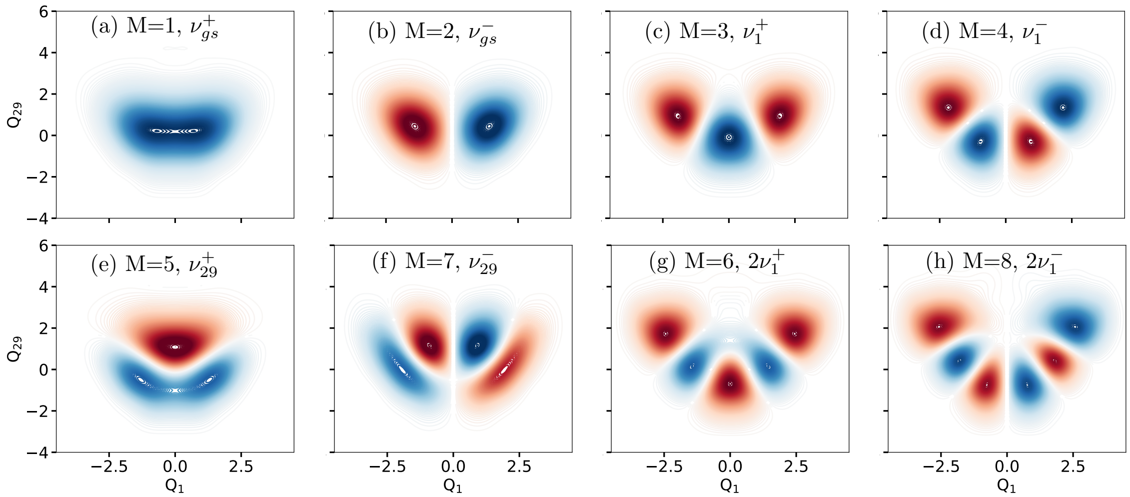

FIG. S3. **Plots of Q_1-Q_{29} eigenstates.** The descriptions of these states are given in Table S4. The labelling is consistent with the nodal pattern in each plot.

TABLE S6. **Two-dimensional eigenstates in Q_1-Q_5 subspace.** The columns follow the description given in Table S2. The $n^\circ\nu_{1,5}^{\pm}$ label only indicates the nth state of a given parity, and is not to be confused with the standard $n\nu_1^{\pm}$ notation.

M	Label	E_M	E_M^{ex}	Δ	Description
1	ν_{gs}^{+}	241.8	0.0		$+0.7566\ 1_{0^+}5_0\ +0.6107\ 1_{1^+}5_0$
2	ν_{gs}^{-}	654.8	413.0	413.0	$+0.5937\ 1_{0^+}5_1\ +0.5722\ 1_{0^-}5_0\ +0.3756\ 1_{1^+}5_1\ +0.2935\ 1_{1^-}5_0$
3	$1^\circ\nu_{1,5}^{-}$	882.8	641.0		$+0.6282\ 1_{0^-}5_0\ -0.4508\ 1_{0^+}5_1\ -0.4088\ 1_{1^+}5_1\ +0.3761\ 1_{1^-}5_0$
4	$1^\circ\nu_{1,5}^{+}$	1047.5	805.7		$+0.5747\ 1_{0^+}5_2\ -0.5652\ 1_{0^-}5_1\ +0.3243\ 1_{1^+}5_2\ -0.2600\ 1_{1^-}5_1$
5	$2^\circ\nu_{1,5}^{+}$	1394.4	1152.6		$+0.5774\ 1_{0^-}5_1\ +0.4393\ 1_{0^+}5_2\ +0.4131\ 1_{1^+}5_2\ +0.3344\ 1_{1^-}5_1$
6	$2^\circ\nu_{1,5}^{-}$	1472.0	1230.2	424.5[a]	$+0.5573\ 1_{0^+}5_3\ +0.5548\ 1_{0^-}5_2\ +0.2820\ 1_{1^+}5_3\ +0.2368\ 1_{1^-}5_2$
7	$3^\circ\nu_{1,5}^{-}$	1872.3	1630.5		$+0.5280\ 1_{0^-}5_2\ -0.4356\ 1_{0^+}5_3\ -0.4237\ 1_{1^+}5_3\ +0.2966\ 1_{1^-}5_2$ $-0.2367\ 1_{0^-}5_3$
8	$3^\circ\nu_{1,5}^{+}$	1912.2	1670.4		$+0.5443\ 1_{0^-}5_3\ +0.5393\ 1_{0^+}5_4\ +0.2450\ 1_{1^+}5_4$
10	$4^\circ\nu_{1,5}^{+}$	2348.6	2106.8		$+0.4787\ 1_{0^-}5_3\ -0.4505\ 1_{0^+}5_4\ -0.4443\ 1_{1^+}5_4\ +0.2591\ 1_{1^-}5_3$ $-0.2529\ 1_{1^+}5_2\ -0.2526\ 1_{0^-}5_4$
11	$4^\circ\nu_{1,5}^{-}$	2375.4	2133.6	463.2[b]	$+0.5480\ 1_{0^-}5_4\ -0.5383\ 1_{0^+}5_5\ -0.2561\ 1_{1^+}5_3$
13	$5^\circ\nu_{1,5}^{-}$	2827.7	2585.9		$+0.4585\ 1_{0^+}5_5\ +0.4577\ 1_{0^+}5_4\ +0.4531\ 1_{1^+}5_5\ -0.2758\ 1_{1^+}5_3$ $+0.2390\ 1_{1^+}5_4$
9	ν_1^{+}	2064.4	1822.6		$+0.6168\ 1_{1^+}5_0\ -0.5308\ 1_{0^+}5_0\ +0.4744\ 1_{2^+}5_0$
19	ν_1^{-}	3482.7	3240.9	1418.3	$+0.6797\ 1_{1^-}5_0\ -0.4808\ 1_{2^-}5_0\ -0.4336\ 1_{0^-}5_0$
12	$(\nu_1+\nu_5)^{+}$	2545.2	2303.4		$+0.5924\ 1_{1^+}5_1\ -0.4793\ 1_{0^+}5_1\ +0.4014\ 1_{2^+}5_1\ -0.2465\ 1_{1^-}5_2$ $+0.2237\ 1_{1^-}5_0$
15	$(\nu_1+2\nu_5)^{+}$	2974.4	2732.6		$+0.5449\ 1_{1^+}5_2\ -0.4471\ 1_{0^+}5_2\ +0.3387\ 1_{2^+}5_2\ -0.3012\ 1_{1^-}5_1$ $+0.2994\ 1_{1^-}5_3$
18	$(\nu_1+3\nu_5)^{+}$	3412.1	3170.3		$+0.5044\ 1_{1^+}5_3\ -0.4209\ 1_{0^+}5_3\ +0.3387\ 1_{1^-}5_4\ +0.3346\ 1_{1^-}5_2$ $+0.2886\ 1_{2^+}5_3$

[a,b] Possible tunneling pair with M=4 and M=8, respectively.

states are difficult to be attributed purely Q_1 or Q_{29} excitations, respectively. One possible reason could be the similar frequencies of Q_1 and Q_{29} (2759.5 cm^{-1}, 2270.7 cm^{-1}) at the local minimum of Q_1-Q_{29} 2D potential. The tunneling splitting pattern reveals an enhancement in tunneling due to Q_{29} excitation as well but this is difficult to attribute solely to Q_{29} as most states have some Q_1 contribution as well.

TABLE S7. **Convergence of Q_1-Q_5 states.** The states listed match those given in the corresponding table of the manuscript. See the caption of Table S3 for notational details.

M	Label	E_M		Δ		$\lvert\%\Delta_{err}\rvert$
		(18, 12)	(18, 10)	(18, 12)	(18, 10)	
1	ν_{gs}^+	241.83	241.26			
2	ν_{gs}^-	654.79	654.99	412.96	413.73	0.19
3	$1^\circ\nu_{1,5}^-$	882.77	882.97			
4	$1^\circ\nu_{1,5}^+$	1047.49	1047.25			
5	$2^\circ\nu_{1,5}^+$	1394.35	1394.26			
6	$2^\circ\nu_{1,5}^-$	1471.96	1471.46	424.47[a]	424.21[a]	0.06
7	$3^\circ\nu_{1,5}^-$	1872.33	1871.33			
8	$3^\circ\nu_{1,5}^+$	1912.16	1913.20			
10	$4^\circ\nu_{1,5}^+$	2348.57	2348.34			
11	$4^\circ\nu_{1,5}^-$	2375.39	2371.82	463.23[b]	458.62[b]	1.00
13	$5^\circ\nu_{1,5}^-$	2827.69	2825.13			
9	ν_1^+	2064.37	2064.04			
19	ν_1^-	3482.71	3482.57	1418.34	1418.53	0.01
12	$(\nu_1+\nu_5)^+$	2545.18	2545.87			
15	$(\nu_1+2\nu_5)^+$	2974.40	2974.07			
18	$(\nu_1+3\nu_5)^+$	3412.11	3406.83			

[a,b] Possible tunneling pair with M=4 and M=8, respectively.

3. Q_1-Q_5 *Eigenstates*

Q_5 is the only other B_2 mode apart from Q_1 in the seven mode subspace, and hence the Q_1-Q_5 potential is of the asymmetrically coupled type. The effective barrier height in the Q_1-Q_5 2D potential is about 565 cm^{-1}. The computed eigenstates are given in Table S6 and their plots are in Figure S4. Owing to asymmetry and weak coupling, which is evident from the small shift of the two minima in the Q_5 direction in Fig. 5a, nodal lines are along the diagonal and antidiagonal. For some higher energy states, though, nodal lines become almost parallel to Q_1 axis, as predicted in the model calculation by Takada and Nakamura[8] and making them easier to assign than other states. In all cases, the parity assignment arises from the presence/absence of sign change to the $(Q_1, Q_5) \to (-Q_1, -Q_5)$ transformation.

The lowest two states are $\nu_{gs}^{\pm}$. State $M = 9$ and 19 have one quantum of excitation in Q_1, which is evident from nodal structure. These are assigned ν_1^+ and ν_1^-. Other clearly identifiable states are $M = 12$, 15, and 18, which are of overall positive parity and readily assigned to $(\nu_1 + n\nu_5)^+$, $n = 1-3$. Based on the size of the $\nu_1^{\pm}$ splitting, their tunneling pair states are expected to be in the 4000-5000 cm^{-1} range.

Other listed states are not easily attributed to excitation in a particular mode. Only their parity is clear. Hence the states are labelled as $n^\circ\nu_{1,5}^{\pm}$, where n is just a serial index for a state of that parity. It must be emphasized that this n does not refer to the number of quanta. As shown in Fig. S4, the nodal lines are either along the diagonal or antidiagonal. Consider first the set of states $M = 4$, 6, 8, and 11, whose nodes are along the diagonal. It is tempting to assign the M pairs (4, 6) and (8, 11) as tunneling doublets. The wavefunctions are evidently spread along the IRC path in this 2D space. Simple $\pm$ linear combinations within each pair are found to be localized in one well or the other, and a wavepacket propagation initiated with these localized packets (implemented through the split operator method) shows that the evolving packet proceeds *through* the diagonal. With support from these observations, splittings for these pairs are given in Table S6. Compared to that for the $\nu_{gs}^{\pm}$ pair, these pairs show increasing splitting. However, the increase is modest compared to that seen for increasing Q_{10} excitation in Table S2.

The other set is made of $M = 3$, 5, 7, 10, and 13. These states have increasing number of antidiagonal nodes. It is unclear that these can be organized as tunneling pairs. For example, wavepacket dynamics initiated with the $\pm$ linear combination of $M = 3$ and 5 evolved from a localized on the bottom left region to the top right region while always having a node along the antidiagonal. The significance of such observations in the context of tunneling dynamics is not immediately apparent.

It is instructive to contrast the present results with the ASMC model of Takada and Nakamura.[7,8] Correcting for

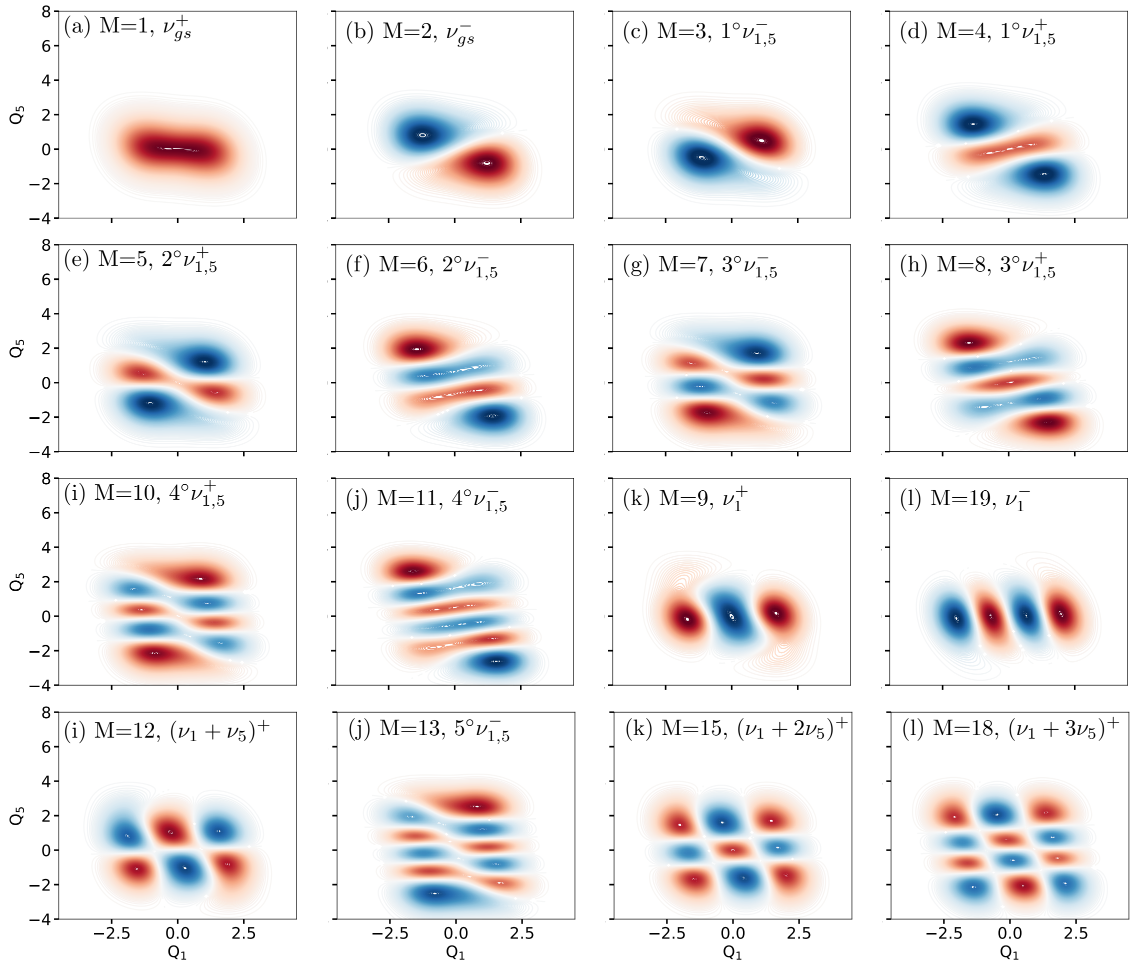

FIG. S4. **Plots of Q_1-Q_5 eigenstates.** The descriptions of these states are given in Table S6. The labelling is consistent with the nodal pattern in each plot.

mode signs between their model and ours, the antidiagonal regions (second and fourth quadrants, hence between the wells) and the diagonal regions (first and third quadrants) belong to the regions of complex (C) and imaginary (I) actions, respectively. The small shift of minimum and low frequency of Q_5 indicate the weak coupling regime, which corresponds to the ASMC case with overlapping C regions associated with the two wells. Prior calculations[7,8] used localized wavefunctions with quanta of excitation directly along the low frequency mode, and mixed tunneling was predicted to take place through the C regions. Their numerical results showed an oscillating pattern of tunneling splittings. In the present instance, an approximate comparison may be made with the linear combinations of pairs (4, 6) and (8, 11), where the wavepacket dynamics does show tunneling though the C region. If indeed these pairs are tunneling doublets, we see simple enhancement of tunneling. In contrast, the states $M = 3$, 5, 7, 10, and 13 do not appear to have a direct counterpart with the Takada-Nakamura work. In a limiting perspective, this set of states may be considered as ones with increasing quanta perpendicular to the tunneling direction. Also, as mentioned just above, dynamics from linear combinations of these states, such as $M = 3$ and 5, are not so revealing.

4. Q_1-Q_x *Eigenstates,* $x = 7$*, 13, 27*

The trio of A_1 modes Q_7, Q_{13}, and Q_{27} form the next rung of modes relevant to the H-transfer (after Q_1, Q_5, Q_{10} and Q_{29}.) Their displacement from TS to EQM contributes about 150 cm^{-1} towards reaching the actual minimum (see Section 2.1 of the manuscript) indicating their minor energetic relevance compared to the four key modes. The minimal nature of their coupling to the transfer mode is evident from their 2D potentials with Q_1 in Fig. 5 of the manuscript. This is not suprising given that the motions (see Fig. 2 of manuscript) involve the ring structural changes that accompany the H atom transfer. The barrier heights in the Q_1-Q_x spaces are about ($x = 7$) 542 cm^{-1}, ($x = 13$) 542

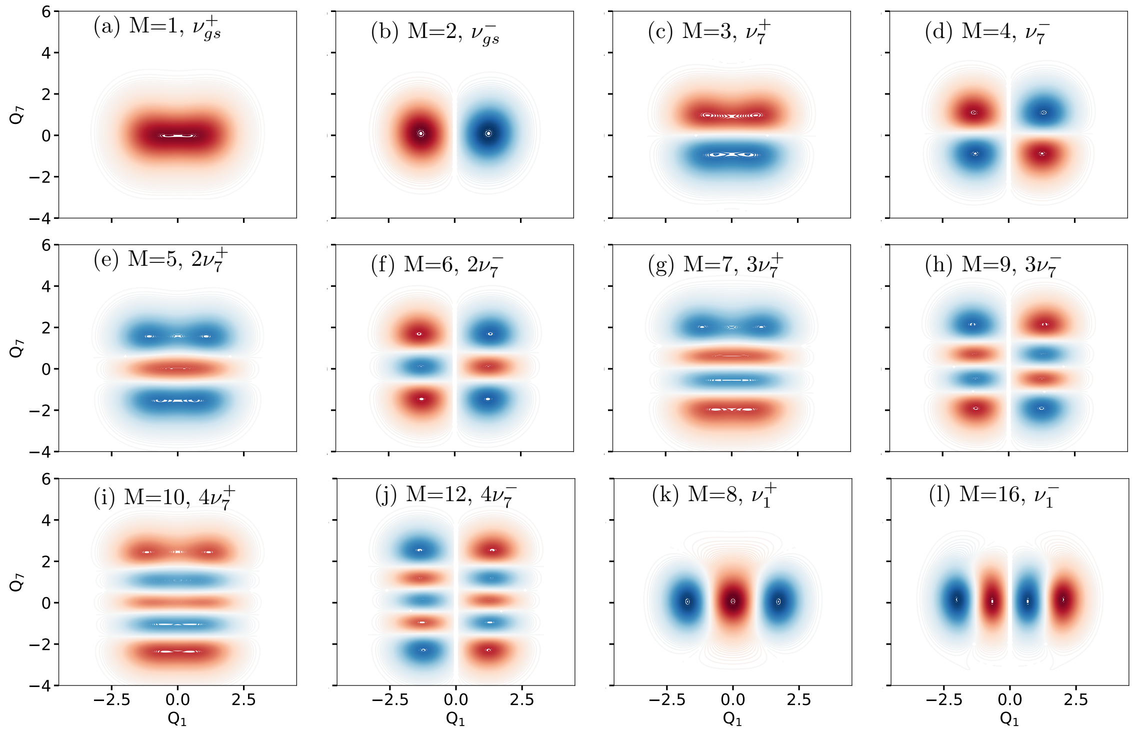

FIG. S5. **Plots of Q_1-Q_7 eigenstates.** The descriptions of these states are given in Table S8. The labelling is consistent with the nodal pattern in each plot.

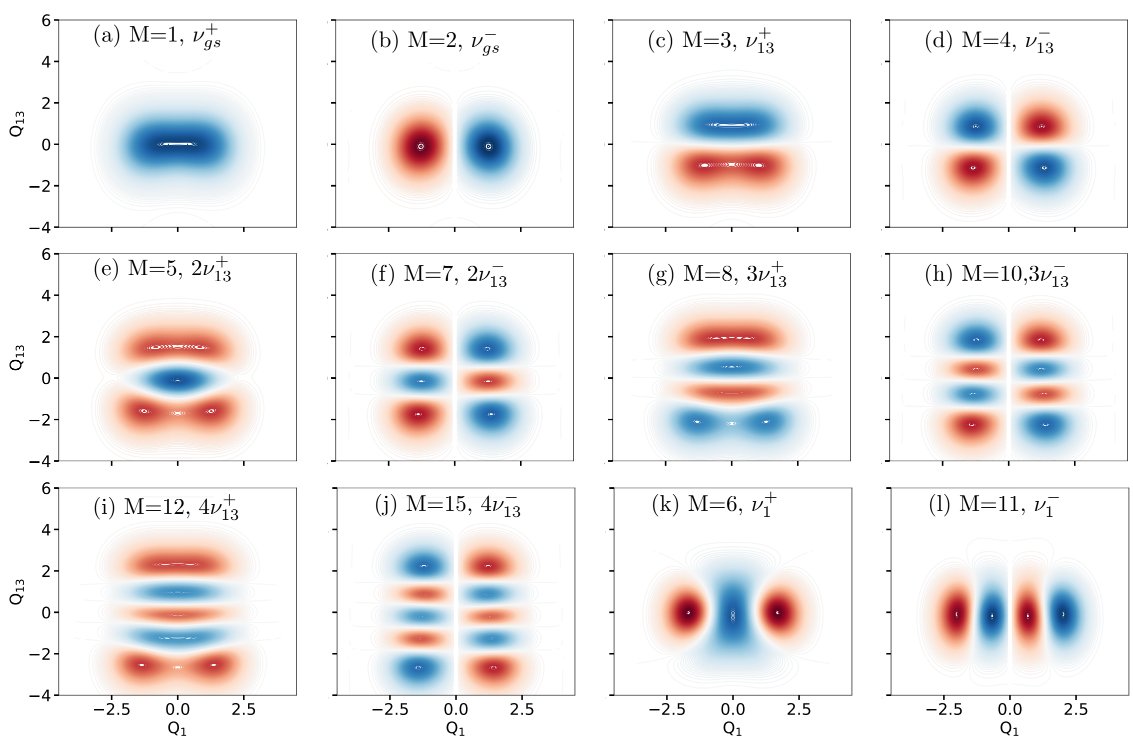

FIG. S6. **Plots of Q_1-Q_{13} eigenstates.** The descriptions of these states are given in Table S10. The labelling is consistent with the nodal pattern in each plot.

TABLE S8. **Two-dimensional eigenstates in Q_1-Q_7 subspace,** their description, assignment, and tunneling splittings. The columns follow those of Table IV for Q_1-Q_{10} states in the manuscript.

M	Label	E_M	E_M^{ex}	Δ	Description
1	ν_{gs}^+	302.0	0.0		$+0.7693\ 1_{0^+}7_0\ \ +0.6331\ 1_{1^+}7_0$
2	ν_{gs}^-	841.0	539.0	539.0	$+0.8679\ 1_{0^-}7_0\ \ +0.4927\ 1_{1^-}7_0$
3	ν_7^+	925.7	623.7		$+0.7846\ 1_{0^+}7_1\ \ +0.6079\ 1_{1^+}7_1$
4	ν_7^-	1412.2	1110.2	486.5	$+0.8716\ 1_{0^-}7_1\ \ +0.4859\ 1_{1^-}7_1$
5	$2\nu_7^+$	1486.0	1184.0		$+0.7811\ 1_{0^+}7_2\ \ +0.6003\ 1_{1^+}7_2$
6	$2\nu_7^-$	1968.1	1666.1	482.1	$+0.8719\ 1_{0^-}7_2\ \ +0.4844\ 1_{1^-}7_2$
7	$3\nu_7^+$	2035.5	1733.5		$+0.7791\ 1_{0^+}7_3\ \ +0.5995\ 1_{1^+}7_3$
9	$3\nu_7^-$	2521.0	2219.0	485.5	$+0.8717\ 1_{0^-}7_3\ \ +0.4836\ 1_{1^-}7_3$
10	$4\nu_7^+$	2613.2	2311.2		$+0.7812\ 1_{0^+}7_4\ \ +0.5895\ 1_{1^+}7_4$
12	$4\nu_7^-$	3083.5	2781.5	470.3	$+0.8729\ 1_{0^-}7_4\ \ +0.4806\ 1_{1^-}7_4$
8	ν_1^+	2105.1	1803.1		$+0.6534\ 1_{1^+}7_0\ \ -0.5495\ 1_{0^+}7_0\ \ +0.5049\ 1_{2^+}7_0$
16	ν_1^-	3506.6	3204.6	1401.5	$+0.7259\ 1_{1^-}7_0\ \ -0.5146\ 1_{2^-}7_0\ \ -0.4460\ 1_{0^-}7_0$

TABLE S9. **Convergence of Q_1-Q_7 states.** The states listed match those given in Table S8 just above. See the caption of Table S3 for notational details. For some states, the index of the correct state in the lower basis (identified visually from eigenstate plots) is different from that in the higher basis. For such cases, a second M value from the lower basis calculation is given in parentheses.

M	Label	E_M		Δ		$\lvert\%\Delta_{err}\rvert$
		(18, 8)	(18, 6)	(18, 8)	(18, 6)	
1	ν_{gs}^+	301.95	301.63			
2	ν_{gs}^-	840.99	841.35	539.04	539.72	0.13
3	ν_7^+	925.67	921.06			
4	ν_7^-	1412.18	1410.75	486.51	489.69	0.65
5	$2\nu_7^+$	1485.99	1492.35			
6	$2\nu_7^-$	1968.09	1970.05	482.10	477.70	0.91
7	$3\nu_7^+$	2035.48	2024.96			
9 (10)	$3\nu_7^-$	2521.04	2518.82	485.56	493.86	1.71
10 (11)	$4\nu_7^+$	2613.23	2646.08			
12 (14)	$4\nu_7^-$	3083.45	3082.48	470.22	436.40	7.19
8	ν_1^+	2105.12	2104.12			
16	ν_1^-	3506.56	3507.02	1401.44	1402.9	0.10

TABLE S10. **Two-dimensional eigenstates in the Q_1-Q_{13} subspace,** their description, assignment, and tunneling splittings. The columns follow those of Table IV for Q_1-Q_{10} states in the manuscript.

M	Label	E_M	E_M^{ex}	Δ	Description
1	ν_{gs}^+	421.2	0.0		$+0.7702\ 1_{0^+}13_0\ \ +0.6320\ 1_{1^+}13_0$
2	ν_{gs}^-	958.1	536.9	536.9	$+0.8687\ 1_{0^-}13_0\ \ +0.4913\ 1_{1^-}13_0$
3	ν_{13}^+	1282.1	860.9		$+0.7854\ 1_{0^+}13_1\ \ +0.6016\ 1_{1^+}13_1$
4	ν_{13}^-	1764.0	1342.8	481.9	$+0.8732\ 1_{0^-}13_1\ \ +0.4821\ 1_{1^-}13_1$
5	$2\nu_{13}^+$	2061.1	1639.9		$+0.7491\ 1_{0^+}13_2\ \ +0.5731\ 1_{1^+}13_2$
7	$2\nu_{13}^-$	2550.0	2128.8	488.9	$+0.8737\ 1_{0^-}13_2\ \ +0.4787\ 1_{1^-}13_2$
8	$3\nu_{13}^+$	2866.2	2445.0		$+0.7732\ 1_{0^+}13_3\ \ +0.5798\ 1_{1^+}13_3$
10	$3\nu_{13}^-$	3342.0	2920.8	475.8	$+0.8753\ 1_{0^-}13_3\ \ +0.4741\ 1_{1^-}13_3$
12	$4\nu_{13}^+$	3646.9	3225.7		$+0.7689\ 1_{0^+}13_4\ \ +0.5709\ 1_{1^+}13_4$
15	$4\nu_{13}^-$	4123.6	3702.4	476.7	$+0.8747\ 1_{0^-}13_4\ \ +0.4708\ 1_{1^-}13_4$
6	ν_1^+	2238.9	1817.7		$+0.6316\ 1_{1^+}13_0\ \ -0.5194\ 1_{0^+}13_0\ \ +0.4815\ 1_{2^+}13_0\ \ -0.2412\ 1_{0^+}13_2$
11	ν_1^-	3622.8	3201.6	1383.9	$+0.7275\ 1_{1^-}13_0\ \ -0.5131\ 1_{2^-}13_0\ \ -0.4447\ 1_{0^-}13_0$

cm^{-1}, and ($x = 27$) 546 cm^{-1}. Tables S8, S10 and S12 below list the eigenvalues, descriptions and tunneling splittings in these 2D spaces, while the corresponding eigenstate plots are in Figs. S5, S6, and S7. Convergence data are given in Tables S9, S11 and S13.

As these tables and plots show, the assignments of eigenstates in term of excitations in Q_7, Q_{13} and Q_{27} is straightforward. The tunneling doublets for all three Q_1-Q_x spaces all exhibit a similar pattern of mode-specific excitation.

TABLE S11. **Convergence of Q_1-Q_{13} states.** The states listed match those given in Table S10 just above. See the caption of Table S3 for notational details. For some states, the index of the correct state in the lower basis (identified visually from eigenstate plots) is different from that in the higher basis. For such cases, a second M value from the lower basis calculation is given in parentheses.

M	Label	E_M		Δ		$\|\%\Delta_{err}\|$
		(18, 7)	(18, 6)	(18, 7)	(18, 6)	
1	ν_{gs}^+	421.22	424.63			
2	ν_{gs}^-	958.11	958.64	536.89	534.01	0.54
3	ν_{13}^+	1282.13	1281.27			
4	ν_{13}^-	1763.99	1763.04	481.86	481.77	0.02
5	$2\nu_{13}^+$	2061.09	2068.36			
7	$2\nu_{13}^-$	2549.99	2553.34	488.90	484.98	0.80
8	$3\nu_{13}^+$	2866.21	2852.12			
10 (11)	$3\nu_{13}^-$	3342.02	3335.75	475.81	483.63	1.64
12 (14)	$4\nu_{13}^+$	3646.87	3745.44			
15 (16)	$4\nu_{13}^-$	4123.60	4134.31	476.73	388.87	18.43
6	ν_1^+	2238.90	2239.60			
11 (12)	ν_1^-	3622.79	3623.89	1383.89	1384.29	0.03

TABLE S12. **Two-dimensional eigenstates in the Q_1-Q_{27} subspace**, their description, assignment, and tunneling splittings. The columns follow those of Table IV for Q_1-Q_{10} states in the manuscript.

M	Label	E_M	E_M^{ex}	Δ	Description
1	ν_{gs}^+	806.6	0.0		$+0.7736\ 1_{0^+}27_0\ \ +0.6320\ 1_{1^+}27_0$
2	ν_{gs}^-	1341.0	534.4	534.4	$+0.8704\ 1_{0^-}27_0\ \ +0.4868\ 1_{1^-}27_0$
3	ν_{27}^+	2410.4	1603.8		$+0.7341\ 1_{0^+}27_1\ \ +0.5326\ 1_{1^+}27_1\ \ -0.2795\ 1_{1^+}27_0\ \ +0.2411\ 1_{0^+}27_0$
5	ν_{27}^-	2921.6	2115.0	511.2	$+0.8715\ 1_{0^-}27_1\ \ +0.4686\ 1_{1^-}27_1$
7	$2\nu_{27}^+$	4004.5	3197.9		$+0.7464\ 1_{0^+}27_2\ \ +0.5135\ 1_{1^+}27_2\ \ -0.2977\ 1_{1^+}27_1\ \ +0.2253\ 1_{0^+}27_1$
9	$2\nu_{27}^-$	4500.5	3693.9	496.0	$+0.8706\ 1_{0^-}27_2\ \ +0.4564\ 1_{1^-}27_2$
4	ν_1^+	2621.9	1815.3		$+0.5970\ 1_{1^+}27_0\ \ -0.4991\ 1_{0^+}27_0\ \ +0.4585\ 1_{2^+}27_0\ \ +0.3050\ 1_{1^+}27_1\ \ +0.2941\ 1_{0^+}27_1$
6	ν_1^-	3987.6	3181.0	1365.7	$+0.7253\ 1_{1^-}27_0\ \ -0.4980\ 1_{2^-}27_0\ \ -0.4390\ 1_{0^-}27_0$

TABLE S13. **Convergence of Q_1-Q_{27} states.** The states listed match those given in Table S12 just above. See the caption of Table S3 for notational details. For some states, the index of the correct state in the lower basis (identified visually from eigenstate plots) is different from that in the higher basis. For such cases, a second M value from the lower basis calculation is given in parentheses.

M	Label	E_M		Δ		$\|\%\Delta_{err}\|$
		(18, 6)	(18, 5)	(18, 6)	(18, 5)	
1	ν_{gs}^+	806.61	811.21			
2	ν_{gs}^-	1341.01	1339.97	534.40	528.76	1.06
3	ν_{27}^+	2410.37	2424.47			
5	ν_{27}^-	2921.63	2927.22	511.26	502.75	1.66
7 (6)	$2\nu_{27}^+$	4004.51	3980.64			
9	$2\nu_{27}^-$	4500.54	4493.08	496.03	512.44	3.31
4	ν_1^+	2621.91	2629.72			
6 (7)	ν_1^-	3987.60	3986.45	1365.69	1356.73	0.66

Excitation in Q_1 increases the tunneling splitting as expected, while there is a *decrease* in splitting of about 30-60 cm^{-1} upon excitation in Q_x where $x = 7, 13, 27$. This can be attributed to minimal coupling of these modes to Q_1, whereby excitation in Q_x leads to increase in amplitude in a direction almost orthogonal to Q_1, where the barriers are higher and less conducive to tunneling. For a better understanding, we revisit these potentials in Sec. III A 5 below with a sudden approximation calculation.

5. *Sudden approximation analysis in 2D subspaces*

Having computed variational eigenstates in various 2D subspaces, we analyse whether tunneling splittings from an approximate method also shows similar trends. In particular, we use the sudden approximation, which provides insights into the role of coupling strength and local frequency in tunneling. As used in the literature, this approximation considers the reaction coordinate (here Q_1) as the fast (high frequency) variable, so the other slow (low frequency) coordinates can be held fixed or controlled. The essence of this approach stems from this separation of frequencies. In the present context, an estimate of tunneling splittings can be obtained within this framework.

We limit our analysis to 2D Q_1-Q_y subspaces, where $y = 7$, 10, 13, and 27. Within the treatment of 2D Hamiltonians for tunneling, the frequency of the coupling coordinate is a parameter[8,11,12] but is typically so chosen that it is suffi-

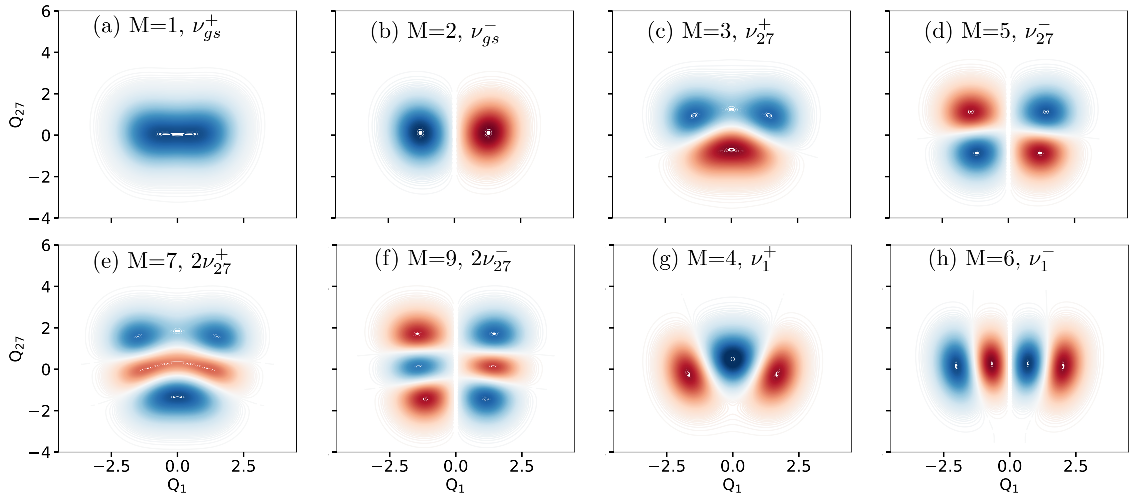

FIG. S7. **Plots of Q_1-Q_{27} eigenstates.** The descriptions of these states are given in Table S12. The labelling is consistent with the nodal pattern in each plot.

TABLE S14. **Local minima and frequencies in 2D Q_1-Q_y subspaces.** Minimum positions and energies in selected subspaces, and the frequencies of both modes at these minima are listed. The frequencies are obtained by 9-point numerical differentiation.

Q_1-Q_y	Q_1^{min}	Q_y^{min}	E_{min} (cm^{-1})	ν_1 (cm^{-1})	ν_y (cm^{-1})
Q_1-Q_7	-1.32	0.10	-541.6	2694.6	578.7
Q_1-Q_{10}	-1.88	1.56	-960.1	4602.8	814.0
Q_1-Q_{13}	-1.32	-0.09	-542.2	2711.7	812.4
Q_1-Q_{27}	-1.33	0.09	-545.7	2671.3	1608.4
Q_1-Q_{29}	-1.48	0.35	-641.8	2759.6	2270.7

TABLE S15. **Tunneling splittings in the sudden approximation.** Ground and vibrationally excited state tunneling splittings Δ_{n_1,n_y} in the Q_1-Q_y spaces ($y = 7$, 10, 13, 27) with this approximation are compared with the results from variational 2D QM calculations (given in parentheses and taken from earlier tables in this ESI).

Δ_{n_1,n_y}	Q_1-Q_7	Q_1-Q_{10}	Q_1-Q_{13}	Q_1-Q_{27}
$\Delta_{0,0}$	534.5 (539.0)	158.7 (241.8)	529.4 (536.9)	532.1 (534.4)
$\Delta_{0,1}$	484.7 (486.5)	206.8 (303.9)	477.6 (481.9)	484.5 (511.3)
$\Delta_{0,2}$	480.3 (482.1)	263.9 (350.5)	470.4 (488.9)	479.9 (496.0)
$\Delta_{0,3}$	478.0 (485.6)	302.5 (394.6)	464.1 (475.8)	478.3 –

ciently smaller than that of the reaction coordinate. In order to check the applicability of the sudden approximation in 2D spaces for catecholate monoanion, we compute the frequencies of Q_1 and Q_y at the local minima in the 2D subspaces. These are given in Table S14. The frequency disparity between them is reasonably applicable in all cases, albeit less so for Q_1-Q_{27} where the frequency ratio is slightly smaller than 0.5. The table additionally lists Q_1-Q_{29}. Given the high frequency ratio and knowing that they are strongly coupled, we do not apply the present analysis to this pair. We also note that satisfactory comparisons for the Q_1-Q_{10} space is not expected as this pair is the most strongly coupled in catecholate monoanion.

The calculation of tunneling splitting in 2D under the sudden approximation has been done by numerical integration of the following formula:[11]

$$\Delta_{n_1,n_y} = \int dQ_y \left[\phi_{n_y}(Q_y|Q_1^{\mathrm{min}})\right]^2 \Delta_{n_1}^{\mathrm{1D}}(Q_y). \tag{1}$$

$\Delta_{n_1}^{\mathrm{1D}}(Q_y)$ is the tunneling splitting along Q_1 at a fixed value of Q_y, while $\phi_{n_y}(Q_y|Q_1^{\mathrm{min}})$ is the 1D eigenfunction along Q_y

TABLE S16. **Three-dimensional eigenstates in Q_1-Q_{10}-Q_{29} subspace, their description, assignment, and tunneling splittings.** The columns follow those of Table S2.

M	Label	E_M	E_M^{ex}	Δ	Description
1	v_{gs}^+	1057.1	0.0		$+0.8545\ 1_{0^+}10_0 29_0$ $+0.2653\ 1_{0^+}10_1 29_0$
2	v_{gs}^-	1139.9	82.8	82.8	$+0.9106\ 1_{0^-}10_0 29_0$
3	v_{10}^+	1374.8	317.7		$+0.6057\ 1_{0^+}10_1 29_0$ $+0.3198\ 1_{1^+}10_0 29_0$ $-0.2849\ 1_{0^+}10_0 29_0$
					$+0.2666\ 1_{1^+}10_2 29_0$ $-0.2506\ 1_{0^+}10_3 29_0$ $+0.2414\ 1_{0^+}10_2 29_0$
4	v_{10}^-	1552.4	495.3	177.6	$+0.8019\ 1_{0^-}10_1 29_0$ $+0.2466\ 1_{1^-}10_0 29_0$ $+0.2256\ 1_{1^-}10_2 29_0$
5	$2v_{10}^+$	1754.6	697.5		$+0.4231\ 1_{0^+}10_2 29_0$ $-0.4029\ 1_{0^+}10_1 29_0$ $+0.2850\ 1_{1^+}10_1 29_0$
					$-0.2824\ 1_{1^+}10_3 29_0$ $-0.2475\ 1_{0^+}10_4 29_0$ $-0.2328\ 1_{0^+}10_0 29_0$
6	$2v_{10}^-$	1993.7	936.6	239.1	$+0.7042\ 1_{0^-}10_2 29_0$ $-0.2688\ 1_{1^-}10_3 29_0$ $+0.2572\ 1_{1^-}10_1 29_0$
7	$3v_{10}^+$	2169.0	1111.9		$+0.3671\ 1_{0^+}10_2 29_0$ $+0.3312\ 1_{0^+}10_3 29_0$ $+0.2808\ 1_{1^+}10_0 29_0$
					$+0.2754\ 1_{1^+}10_4 29_0$ $+0.2409\ 1_{0^+}10_5 29_0$
9	$3v_{10}^-$	2446.8	1389.7	277.8	$+0.6185\ 1_{0^-}10_3 29_0$ $+0.2939\ 1_{1^-}10_4 29_0$ $+0.2547\ 1_{0^-}10_1 29_0$
					$+0.2399\ 1_{0^-}10_5 29_0$ $-0.2385\ 1_{1^-}10_2 29_0$
10	$4v_{10}^+$	2613.7	1556.6		$+0.3464\ 1_{0^+}10_3 29_0$ $-0.2664\ 1_{1^+}10_5 29_0$ $-0.2583\ 1_{0^+}10_4 29_0$
					$+0.2348\ 1_{0^+}10_6 29_0$ $-0.2316\ 1_{1^+}10_1 29_0$
13	$4v_{10}^-$	2917.4	1860.3	303.7	$+0.5465\ 1_{0^-}10_4 29_0$ $+0.3074\ 1_{1^-}10_5 29_0$ $+0.2689\ 1_{0^-}10_2 29_0$
					$-0.2521\ 1_{0^-}10_6 29_0$
8	v_1^+	2384.3	1327.2		$+0.5620\ 1_{1^+}10_0 29_0$ $-0.3789\ 1_{0^+}10_1 29_0$ $+0.3634\ 1_{0^+}10_0 29_1$
					$+0.3365\ 1_{1^+}10_1 29_0$ $-0.2628\ 1_{0^+}10_2 29_0$
11	v_1^-	2655.0	1597.9	270.7	$+0.5274\ 1_{0^-}10_0 29_1$ $+0.5120\ 1_{1^-}10_0 29_0$ $-0.3370\ 1_{0^-}10_1 29_0$
					$+0.2719\ 1_{0^-}10_0 29_0$

at fixed $Q_1 = Q_1^{\min}$ of the 2D space. This approach was used previously for tropolone.[8,11] As the purpose here is to only check the approximation, we focus of the ground tunneling splitting along Q_1.

Some technical details are in order. The 1D eigenfunctions $\phi_{n_y}(Q_y|Q_1^{\min})$ are computed with a HO-DVR basis. For the numerical integration in Eq. (1), a grid of 101 points in Q_y was chosen. These span the range $[-4, 4]$ for Q_7, Q_{13} and Q_{27}, while a wider $[-4, 6]$ range was used for Q_{10}. These ranges were chosen using the corresponding states from the 2D variational calculations. At each value of Q_y, we first do a 1D sinc-DVR calculation along Q_1 in the range $[-4.8, 4.8]$ to get its ground state tunneling splitting $\Delta_0^{\mathrm{1D}}(Q_y)$. The final integral was calculated with Simpson's 1/3rd and trapezoidal methods using Numpy's numerical integration routine.[13] The resulting estimates of tunneling splittings for $n_y =$ 0-3 are listed in Table S15.

The sudden approximation expectedly obtains the correct pattern and reasonably close tunneling splitting values with respect to exact results for minimally coupled potentials involving Q_7, Q_{13} and Q_{27}. While the pattern of increasing splitting for Q_{10} excitation is still captured by the approximation, it strongly underestimates the splitting magnitudes; this may be attributed to the method not accounting for the significant wavefunction amplitude in the curved region with increasing Q_{10} excitation. The importance of curvature in tunneling has been well-discussed in the literature.[9,12] For minimally coupled cases the curvature is small, and the tunneling and IRC paths almost coincide. But for large curvature IRC paths, ignoring the curvature leads to erroneous results.

B. 3D $Q_1 - Q_{10} - Q_{29}$ Eigenstates

The modes Q_1, Q_{10}, and Q_{29} make up a significant reduced dimensional subspace owing to their energetic contribution as a trio (about 3/4$^{\text{th}}$ of the full barrier) and displacement magnitudes shown in Table 1. We present eigenstates in this 3D subspace below. The barrier height in 3D is about 1296 cm^{-1}. The computed eigenstates, their descriptions, and tunneling splittings for different mode specific excitations are listed in Table S16. The convergence behaviour is given in Table S17. The corresponding eigenstate contour plots are provided in Fig. S8. The 3D eigenstates have a more mixed character compared to 2D ones. This indicates strong intermode coupling among Q_1, Q_{10}, and Q_{29}. The structures of the eigenstates show that they are not a mere extension of the respective 2D states discussed further above, although some comparisons may be drawn.

The first two states are of course the ground state pair with a tunneling splitting of 82.8 cm^{-1}. This is considerably smaller than that in the 2D calculations, which may be attributed in part to the to higher barrier in 3D. The states $M = 8$ and $M = 11$ are labelled as the tunneling split pair having one quantum of excitation of Q_1. The splitting of this

TABLE S17. **Convergence of Q_1-Q_{10}-Q_{29} states.** See the caption of Table S3 for notational details.

M	Label	E_M		Δ		$\lvert\%\Delta_{err}\rvert$
		(18, 17, 7)	(18, 15, 6)	(18, 17, 7)	(18, 15, 6)	
1	ν_{gs}^+	1057.05	1056.67			
2	ν_{gs}^-	1139.89	1139.34	82.84	82.67	0.21
3	ν_{10}^+	1374.84	1373.84			
4	ν_{10}^-	1552.38	1552.46	177.54	178.62	0.61
5	$2\nu_{10}^+$	1754.55	1753.89			
6	$2\nu_{10}^-$	1993.69	1994.31	239.14	240.42	0.54
7	$3\nu_{10}^+$	2168.96	2168.32			
9	$3\nu_{10}^-$	2446.78	2447.58	277.82	279.26	0.52
10	$4\nu_{10}^+$	2613.69	2613.39			
13	$4\nu_{10}^-$	2917.43	2917.73	303.74	304.34	0.20
8	ν_1^+	2384.26	2383.29			
11	ν_1^-	2655.02	2655.62	270.76	272.33	0.58

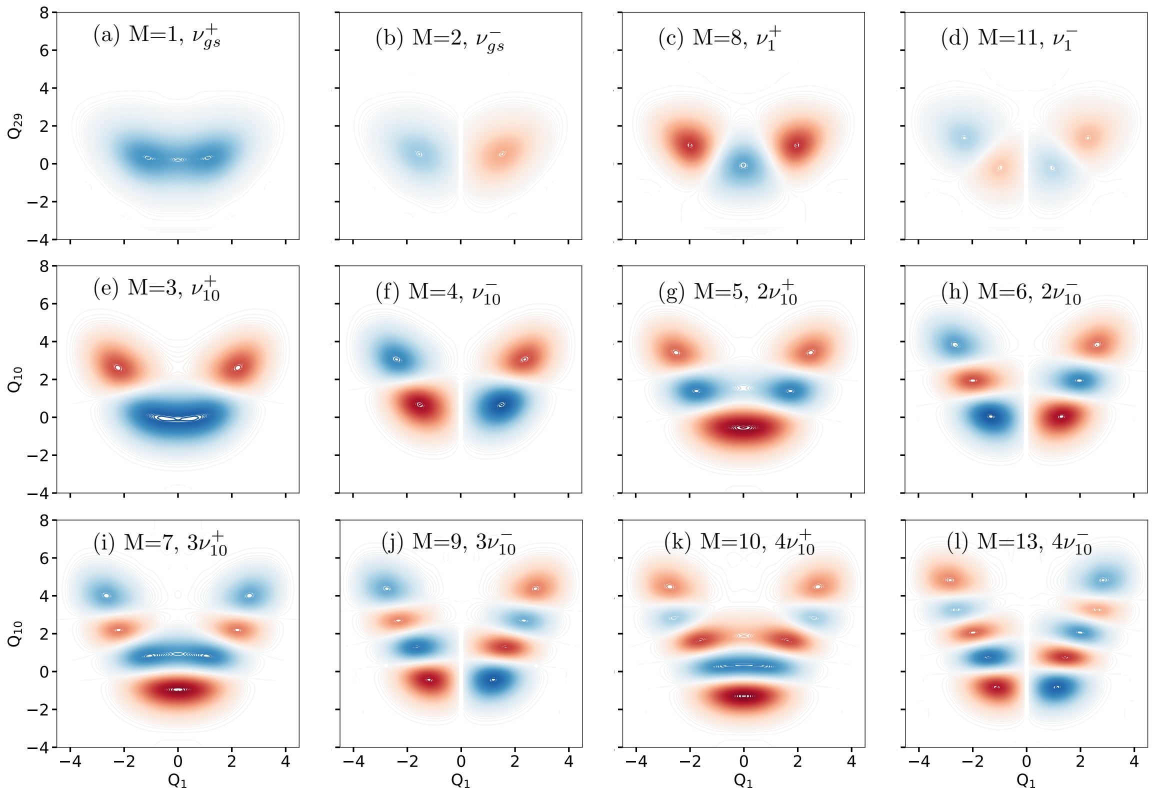

FIG. S8. **Plots of Q_1-Q_{10}-Q_{29} 3D eigenstates.** The descriptions of these states are given in Table VII of the manuscript. The labelling is consistent with the nodal pattern in each plot. In keeping with the text in Section III C of the manuscript, the y-axis in plots (a)-(d) is Q_{29}, while it is Q_{10} in the rest.

excited pair is also much more modest than corresponding values from 2D calculations, again due to the change of barrier height. Yet, the nodal patterns for these two states [Fig. S8(c) and (d)] are very similar to $M = 3$ and $M = 4$ states, respectively, in two dimensional Q_1-Q_{29} calculation. The even parity state ν_1^+ ($M = 8$) has sizeable contribution from direct product states with a total of one quantum in each mode, viz. $1_{1^+}10_0 29_0$, $1_{0^+}10_1 29_0$, $1_{0^+}10_0 29_1$. The odd parity state ν_1^- ($M = 11$) has almost equal contributions from $1_{1^-}10_0 29_0$ and $1_{0^-}10_0 29_1$. In the Q_1-Q_{29} 2D results, similar mixed excitation character in Q_1 and Q_{29} was found.

States pairs $(3, 4)$, $(5, 6)$, $(7, 9)$ and $(10, 13)$ are tunneling doublets due to one, two, three and four quanta of excitation in Q_{10}. These assignments have been done mainly based on nodal patterns. Note also that mode specific excitation in Q_{10} enhances the tunneling splitting, maintaining the trend from Q_1-Q_{10} 2D calculations but with magnitudes lowered due to a higher effective barrier in the present 3D space.

TABLE S18. **Four dimensional eigenstates in Q_1-Q_5-Q_{10}-Q_{29} subspace, their description,assignment, and tunneling splittings.** The columns follow those of Table S2. Some eigenstates are labelled as a/b indicating that both a and b contribute to the description. For certain states involving Q_5, we have expanded the description in terms of the 2D Q_1-Q_5 eigenstates. For these, the subscript of $(1,5)$ refers to the eigenstate serial index from Table S6.

M	Label	E_M	E_M^{ex}	Δ	Description
1	ν_{gs}^+	1286.8	0.0		$+0.8256\ 1_{0^+}5_0 10_0 29_0$ $+0.2509\ 1_{0^+}5_0 10_1 29_0$
2	ν_{gs}^-	1351.1	64.3	64.3	$+0.8576\ 1_{0^-}5_0 10_0 29_0$
3	ν_{10}^+	1612.1	325.3		$+0.5890\ 1_{0^+}5_0 10_1 29_0$ $+0.3097\ 1_{1^+}5_0 10_0 29_0$ $+0.2607\ 1_{0^+}5_0 10_2 29_0$ $+0.2493\ 1_{1^+}5_0 10_2 29_0$ $-0.2442\ 1_{0^+}5_0 10_3 29_0$
4	ν_{10}^-	1758.3	471.5	146.2	$+0.5756\ 1_{0^-}5_0 10_1 29_0$ $+0.4490\ 1_{0^+}5_1 10_0 29_0$ $+0.2869\ 1_{0^+}5_1 10_1 29_0$
5	$\nu_{10}^-/1^\circ\nu_{1,5}^-$	1804.3	517.5		$+0.4859\ (1,5)_3 10_0 29_0$ $+0.4429\ (1,5)_3 10_1 29_0$ $-0.3518\ (1,5)_{12} 10_0 29_0$
7	$2\nu_{10}^+$	2001.6	714.8		$+0.3898\ 1_{0^+}5_0 10_2 29_0$ $-0.3759\ 1_{0^+}5_0 10_1 29_0$ $+0.2771\ 1_{1^+}5_0 10_1 29_0$ $-0.2636\ 1_{1^+}5_0 10_3 29_0$ $-0.2403\ 1_{0^+}5_0 10_4 29_0$ $-0.2375\ 1_{0^+}5_0 10_0 29_0$
10	$2\nu_{10}^-/1^\circ\nu_{1,5}^-$	2252.4	965.6	250.8	$+0.4693\ (1,5)_3 10_2 29_0$ $+0.3238\ (1,5)_2 10_2 29_0$ $+0.2774\ (1,5)_3 10_1 29_0$ $+0.2458\ (1,5)_{19} 10_2 29_0$
13	$3\nu_{10}^+$	2430.5	1143.7		$+0.3722\ 1_{0^+}5_0 10_2 29_0$ $+0.2833\ 1_{0^+}5_0 10_3 29_0$ $+0.2532\ 1_{1^+}5_0 10_0 29_0$ $+0.2507\ 1_{1^+}5_0 10_4 29_0$ $+0.2307\ 1_{0^+}5_0 10_5 29_0$
18	$3\nu_{10}^-$	2722.0	1435.2	291.5	$+0.5092\ 1_{0^-}5_0 10_3 29_0$ $+0.2298\ 1_{1^-}5_0 10_4 29_0$
6	$1^\circ\nu_{1,5}^+$	1834.0	547.2		$+0.5823\ (1,5)_4 10_0 29_0$ $-0.3684\ (1,5)_5 10_0 29_0$ $+0.2264\ (1,5)_4 10_1 29_0$
8	ν_5^-	2109.3	822.5		$+0.3919\ (1,5)_2 10_2 29_0$ $-0.3504\ (1,5)_3 10_1 29_0$ $+0.2760\ (1,5)_2 10_1 29_0$ $-0.2652\ (1,5)_2 10_3 29_0$ $-0.2354\ (1,5)_1 2 10_0 29_0$
9	$1^\circ\nu_{1,5}^+ + \nu_{10}^+$	2233.6	946.8		$+0.5215\ (1,5)_4 10_1 29_0$ $+0.3214\ (1,5)_5 10_0 29_0$ $+0.3005\ (1,5)_4 10_2 29_0$ $+0.2251\ (1,5)_4 10_0 29_0$
11	$2^\circ\nu_{1,5}^+$	2321.1	1034.3		$+0.4652\ (1,5)_5 10_0 29_0$ $+0.4482\ (1,5)_5 10_1 29_0$ $-0.3410\ (1,5)_{15} 10_0 29_0$ $+0.2347\ (1,5)_5 10_2 29_0$
12	$2^\circ\nu_{1,5}^-$	2326.9	1040.1		$+0.5816\ (1,5)_6 10_0 29_0$ $+0.3371\ (1,5)_7 10_0 29_0$ $+0.2821\ (1,5)_6 10_1 29_0$
16	ν_1^+	2657.1	1370.3		$+0.5078\ 1_{1^+}5_0 10_0 29_0$ $+0.3688\ 1_{0^+}5_0 10_0 29_1$ $-0.3390\ 1_{0^+}5_0 10_1 29_0$ $+0.3291\ 1_{1^+}5_0 10_1 29_0$ $-0.2449\ 1_{0^+}5_0 10_2 29_0$
22	ν_1^-	2868.7	1581.9	211.6	$+0.4592\ 1_{0^-}5_0 10_0 29_1$ $+0.4384\ 1_{1^-}5_0 10_0 29_0$ $-0.2933\ 1_{0^-}5_0 10_1 29_0$ $+0.2532\ 1_{0^-}5_0 10_0 29_0$

It can be seen in the next sections that this 3D space sets the template for the analysis of 4D eigenstates in the Q_1-Q_{10}-Q_{29}-Q_x unrelaxed mode spaces, where $x = 5$, 7, 13, and 27.

C. 4D eigenstates

1. Q_1-Q_5-Q_{10}-Q_{29} eigenstates

The barrier height in this important 4D subspace is about 1353 cm^{-1}. Table S18 shows some of the computed states, while the companion Table S19 gives some convergence data. As in lower dimensional subspaces, the state characters are mixed, and we are again aided by nodal patterns shown in Figs. S9 to assign states. Nonetheless, parallels in the eigenstate expansion coefficients are visible, as discussed below.

The first two states are of course the ground state pair $\nu_{gs}^{\pm}$ with a tunneling splitting of 64.3 cm^{-1}, which is a notch lower than the 3D ground state tunneling splitting. Note also that the major expansion coefficients are rather close to those of the ground 3D state pair, except for the presence in 4D of 5_0 in each basis function (compare $\nu_{gs}^{\pm}$ of Table S16). This suggests a minor influence of Q_5 for these states. The plots of both states are shown in the Q_1-Q_{29} space in parts (a) and (b) of Fig. S9. Parts (c) and (d) of the figure show the other easily assigned states, viz. ν_1^+ ($M = 16$) and ν_1^- ($M = 22$). Once again these can be closely matched in plot shape and expansion coefficients with their 3D counterparts. That the major terms do not have any contributions from excited basis function in Q_5 is striking. Some other states also show a similar trend and will be mentioned below. The $\nu_1^{\pm}$ tunneling splitting is about 212 cm^{-1}, which about 20% lower than the 3D value. Before moving to the next set of states, we note that plots for four states just discussed can be compared very well to the 3D eigenstate plots in Figs. S8(a-d), and that replotting them in the Q_1-Q_5 and Q_1-Q_{10} spaces does not reveal any new information.

States $M = 3$, 7 and 13 are readily assigned to ν_{10}^+, $2\nu_{10}^+$ and $3\nu_{10}^+$. These are done on two grounds. First, we

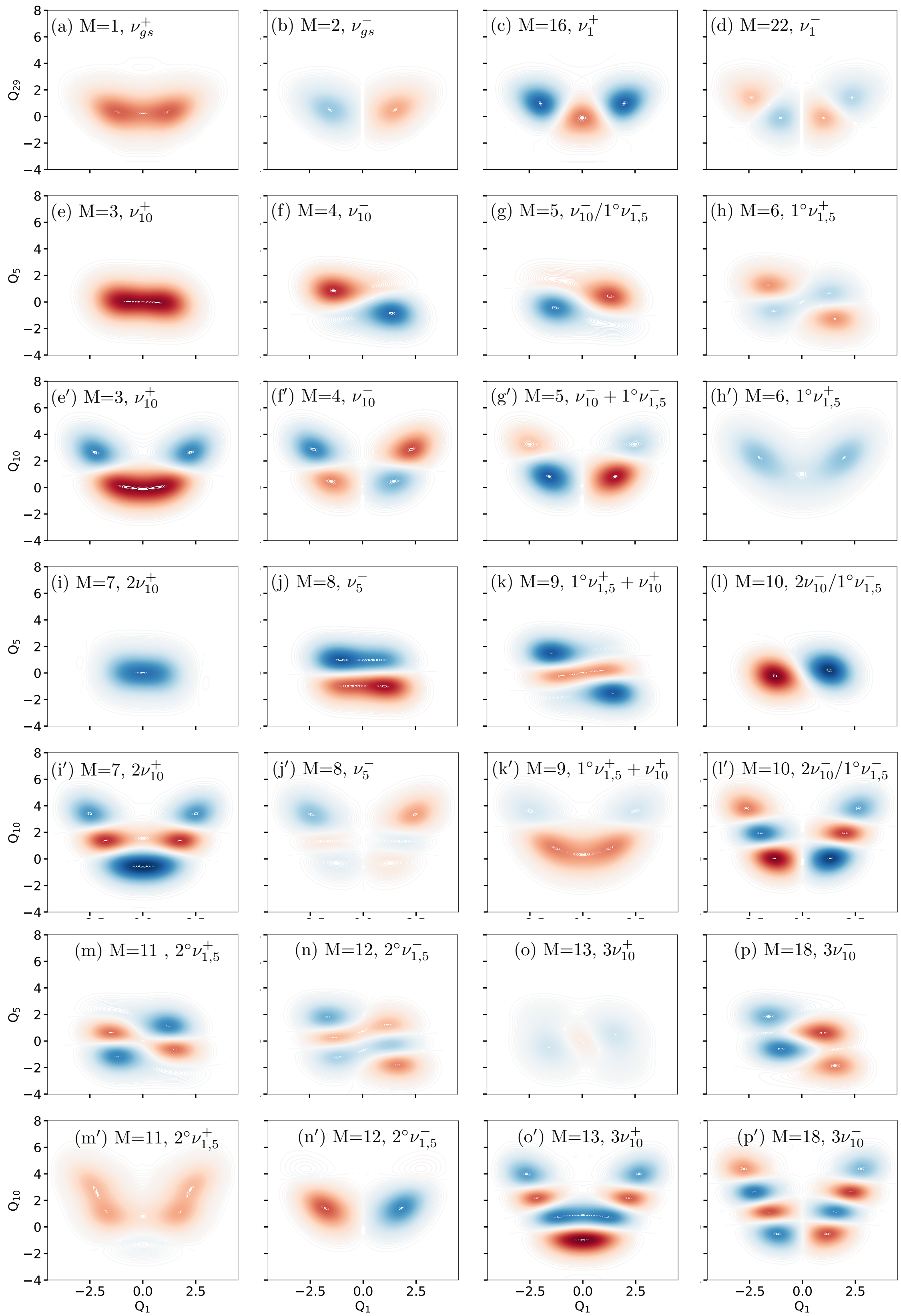

FIG. S9. **Plots of Q_1-Q_5-Q_{10}-Q_{29} eigenstates.** Their descriptions are given in Table S18. Each contour plot is generated from the slice of the wavefunction in the two plotted coordinates at zero values of the other two coordinates.

TABLE S19. **Convergence of Q_1-Q_5-Q_{10}-Q_{29} states.** See the caption of Table S3 for notational details.

M	Label	E_M		Δ		$\|\%\Delta_{err}\|$
		(18, 12, 17, 7)	(18, 10, 15, 6)	(18, 12, 17, 7)	(18, 10, 15, 6)	
1	v_{gs}^{+}	1286.75	1286.61			
2	v_{gs}^{-}	1351.12	1350.71	64.37	64.10	0.42
3	v_{10}^{+}	1612.06	1611.68			
4	v_{10}^{-}	1758.34	1758.39	146.28	146.71	0.29
5	$v_{10}^{-}/1^{\circ}v_{1,5}^{-}$	1804.25	1804.32			
7	$2v_{10}^{+}$	2001.59	2001.15			
10	$2v_{10}^{-}/1^{\circ}v_{1,5}^{-}$	2252.37	2253.02	250.78	251.87	0.43
13	$3v_{10}^{+}$	2430.50	2429.74			
18	$3v_{10}^{-}$	2722.02	2722.55			
6	$1^{\circ}v_{1,5}^{+}$	1834.04	1833.83			
8	v_{5}^{-}	2109.32	2109.09			
9	$1^{\circ}v_{1,5}^{+}+v_{10}^{+}$	2233.61	2233.68			
11	$2^{\circ}v_{1,5}^{+}$	2321.11	2321.26			
12	$2^{\circ}v_{1,5}^{-}$	2326.93	2326.96			
16	v_{1}^{+}	2657.07	2656.50			
22	v_{1}^{-}	2868.74	2869.20	211.67	212.70	0.49

find a term-by-term close match with the major expansion coefficients of corresponding 3D states; compare the corresponding expansions in Table S16. Second is the structure of the wavefunction plots in Figures S9(e, e′), (i, i′) and (o, o′). Note that the unprimed plots are wavefunction slices in Q_1-Q_5 space with $Q_{10} = Q_{29} = 0$, while the primed plots are in Q_1-Q_{10} space with $Q_5 = Q_{29} = 0$. The unprimed slices reveal just the ground state in Q_1-Q_5 space (for v_{10}^{+} and $2v_{10}^{+}$) or a very small contribution of an even parity function (for $3v_{10}^{+}$).

The odd parity counterparts of the above three states are more nuanced. For instance, consider $M = 4$ and 5, which are under 50 cm^{-1} apart. The former has a clear node in Q_{10} and has the same shape as $M = 4$ of the 2D Q_1-Q_{10} space [compare Figs. S9(f′) and S2(d)], while its Q_1-Q_5 slice is much like the 2D v_{gs}^{-} [see Figs. S9(f) and S4(b)]. This prompts the assigment of v_{10}^{-} to this 4D state. Note, however, that its expansion coefficients have some similar terms as its 3D counterpart but with quite different coefficients. The 4D $M = 5$ state also has a similar projection in Q_1-Q_{10} space, and also has a important component of $1^{\circ}v_{1,5}^{-}$ [compare $M = 3$ in Figure S4(c)]. The admixture in $M = 5$ suggests an assignment of $v_{10}^{-}/1^{\circ}v_{1,5}^{-}$, where we use the '$a/b$' shorthand to indicate the presence of both contributions in the eigenstates. Therefore, while we assign $M = 3$ and $M = 4$ as tunneling pairs $v_{10}^{\pm}$, it must be recognized that is not clean pair assignment owing to the nature of $M = 5$. In a similar manner, the states $M = 7$ and 10 can be assigned as the $2v_{10}^{\pm}$ tunneling pairs, but the latter again has $1^{\circ}v_{1,5}^{-}$ mixed in. Likewise, $M = 13$ and $M = 18$ may be assigned as $3v_{10}^{\pm}$ tunneling pairs, while noting that the latter has a new odd parity projection in Q_1-Q_5. Notwithstanding the subtleties in state assignments arising from the mode mixings in 4D, we see a steady increase of tunneling splitting in nv_{10}^{-}, from about ($n = 1$) 146 cm^{-1} to ($n = 2$) 251 cm^{-1} and finally ($n = 3$) 287 cm^{-1}. This continues the trend seen in our 2D and 3D results that the CO scissor motion Q_{10} enhances tunneling.

We note that tunneling doublets due to excitation solely in Q_{29} were not found up to 5000 cm^{-1}, likely due its high frequency as well as inter-mode coupling. It remains to discuss states with dominant excitation in the Q_1-Q_5 subspace. Their assignment is done mainly from nodal patterns. From the 4D contour plots, we directly see that $M = 6$, 11, and 12 have 2D $M = 4$, 5, and 6 in Q_1-Q_5 space as counterparts; see parts (d)-(f) of Fig. S4. The 4D labels are directly derived from the 2D ones. State $M = 9$ appears to be a combination state involving one quantum in Q_{10}. State $M = 8$ has no counterpart in 2D, and appears to be a mainly Q_5 excitation with a small admixture of $2v_{10}^{-}$.

2. $Q_1 - Q_{10} - Q_{29} - Q_x$ *eigenstates with* x*=7, 13, 27*

For the 4D Q_1-Q_{10}-Q_{29}-Q_x subspace, the minimal nature of the coupling with Q_x, $x = 7$, 13, and 27, is suggested by the respective effective barrier heights of about 1319 cm^{-1}, 1330 cm^{-1}, and 1343 cm^{-1} compared to the 3D value (Q_1-Q_{10}-Q_{29}) of 1296 cm^{-1}. Tables S20 (S21), S22 (S23), and S22 (S23) list the 4D eigenstates (and their convergence), while the corresponding plots are in Figs. S10, S12, and S12.

TABLE S20. **Four-dimensional eigenstates in Q_1-Q_7-Q_{10}-Q_{29} subspace, their description,assignment, and tunneling splittings.** The columns follow those of Table IV for Q_1-Q_{10} states in the manuscript. Contour plots for selected states are shown in Fig. S10 below.

M	Label	E_M	E_M^{ex}	Δ	Description
1	ν_{gs}^+	1344.7	0.0		$+0.8612\ 1_{0^+}7_0 10_0 29_0$ $+0.2387\ 1_{0^+}7_0 10_1 29_0$
2	ν_{gs}^-	1410.4	65.7	65.7	$+0.8995\ 1_{0^-}7_0 10_0 29_0$
3	ν_{10}^+	1654.5	309.8		$+0.6237\ 1_{0^+}7_0 10_1 29_0$ $+0.3118\ 1_{1^+}7_0 10_0 29_0$ $+0.2617\ 1_{1^+}7_0 10_2 29_0$
					$-0.2492\ 1_{0^+}7_0 10_3 29_0$ $+0.2370\ 1_{0^+}7_0 10_2 29_0$
4	ν_{10}^-	1813.0	468.3	158.5	$+0.7752\ 1_{0^-}7_0 10_1 29_0$ $+0.2327\ 1_{1^-}7_0 10_0 29_0$
5	ν_7^+	1923.2	578.5		$+0.8442\ 1_{0^+}7_1 10_0 29_0$ $+0.2393\ 1_{0^+}7_1 10_1 29_0$
6	ν_7^-	1980.2	635.5	57.0	$+0.8737\ 1_{0^-}7_1 10_0 29_0$
7	$2\nu_{10}^+$	2021.6	676.9		$+0.4272\ 1_{0^+}7_0 10_2 29_0$ $-0.3404\ 1_{0^+}7_0 10_1 29_0$ $+0.2845\ 1_{1^+}7_0 10_1 29_0$
					$-0.2755\ 1_{1^+}7_0 10_3 29_0$ $-0.2525\ 1_{0^+}7_0 10_0 29_0$ $-0.2428\ 1_{0^+}7_0 10_4 29_0$
9	$2\nu_{10}^-$	2243.0	898.3	221.4	$+0.6581\ 1_{0^-}7_0 10_2 29_0$ $-0.2549\ 1_{1^-}7_0 10_3 29_0$ $+0.2313\ 1_{1^-}7_0 10_1 29_0$
8	$(\nu_7+\nu_{10})^+$	2236.0	891.3		$+0.5957\ 1_{0^+}7_1 10_1 29_0$ $+0.2934\ 1_{1^+}7_1 10_0 29_0$ $+0.2484\ 1_{0^+}7_1 10_2 29_0$
					$+0.2408\ 1_{1^+}7_1 10_2 29_0$ $-0.2397\ 1_{0^+}7_1 10_3 29_0$
10	$(\nu_7+\nu_{10})^-$	2384.0	1039.3	148.0	$+0.7189\ 1_{0^-}7_1 10_1 29_0$
12	$2\nu_7^+$	2487.7	1143.0		$+0.8178\ 1_{0^+}7_2 10_0 29_0$ $+0.2496\ 1_{0^+}7_2 10_1 29_0$
13	$2\nu_7^-$	2545.7	1201.0	58.0	$+0.8495\ 1_{0^-}7_2 10_0 29_0$
11	$3\nu_{10}^+$	2425.7	1081.0		$+0.3203\ 1_{0^+}7_0 10_2 29_0$ $+0.3179\ 1_{0^+}7_0 10_3 29_0$ $+0.2652\ 1_{1^+}7_0 10_4 29_0$
					$+0.2554\ 1_{0^+}7_0 10_1 29_0$ $+0.2325\ 1_{1^+}7_0 10_0 29_0$ $+0.2306\ 1_{0^+}7_0 10_5 29_0$
15	$3\nu_{10}^-$	2684.6	1339.9	258.9	$+0.5523\ 1_{0^-}7_0 10_3 29_0$ $+0.2665\ 1_{1^-}7_0 10_4 29_0$ $+0.2417\ 1_{0^-}7_1 10_2 29_0$
					$+0.2330\ 1_{0^-}7_0 10_1 29_0$
16	ν_1^+	2704.7	1360.0		$+0.5363\ 1_{1^+}7_0 10_0 29_0$ $+0.3761\ 1_{1^+}7_0 10_1 29_0$ $+0.3723\ 1_{0^+}7_0 10_0 29_1$
					$-0.3406\ 1_{0^+}7_0 10_1 29_0$
20	ν_1^-	2940.0	1595.3	235.3	$+0.5229\ 1_{0^-}7_0 10_0 29_1$ $+0.4905\ 1_{1^-}7_0 10_0 29_0$ $-0.3219\ 1_{0^-}7_0 10_1 29_0$
					$+0.2782\ 1_{0^-}7_0 10_0 29_0$
17	$(2\nu_7+\nu_{10})^+$	2801.9	1457.2		$+0.5467\ 1_{0^+}7_2 10_1 29_0$ $+0.2731\ 1_{1^+}7_2 10_0 29_0$ $+0.2606\ 1_{0^+}7_2 10_2 29_0$
					$+0.2304\ 1_{0^+}7_3 10_0 29_0$ $-0.2287\ 1_{0^+}7_2 10_3 29_0$
21	$(2\nu_7+\nu_{10})^-$	2950.9	1606.2	149.0	$+0.6619\ 1_{0^-}7_2 10_1 29_0$ $-0.2834\ 1_{0^-}7_1 10_2 29_0$ $+0.2444\ 1_{0^-}7_3 10_0 29_0$

We compare the present 4D eigenstate descriptions to the 3D Q_1-Q_{10}-Q_{29} states (Table S16). It is readily seen that the five state pairs, $\nu_{gs}^{\pm}$, $\nu_1^{\pm}$, as well as $n\nu_{10}^{\pm}$, $n = 1-3$, are essentially the same as those from the 3D. The dominant direct product eigenstates and their coefficient magnitudes are very similar for these states; of course, each direct product has an additional ground eigenstate along Q_x (i.e. x_0) in them. Excited states of Q_x are not completely absent; for instance, in the Q_7 case, the $3\nu_{10}^-$ state has a small (but larger than 5%) contribution from a direct product that has a 7_1 in it. The roles of Q_x in the above listed states appear overall minor. Corroborating this is the observation that the eigenstate contour plots for the states are like those in 3D. Turning to the tunneling splitting for all five state pairs, we find that while they preserve the patterns found in 3D, their magnitudes are lower than the corresponding 3D values.

In the tables, $n\nu_x^{\pm}$, $n = 1,2$, states are also given. The descriptions of these states indicates a small coupling to Q_{10} (for Q_7 and Q_{13}) and Q_{29} (for Q_{27}). The plots for these states projected onto the Q_1-Q_x space in Figs. S10, S12, and S12 show nodal lines that are essentially parallel to the axes. The tunneling splittings for these states preserve the patterns seen in the 2D Q_1-Q_x calculations, namely a reduction of the tunneling splitting with increase in number of quanta along Q_x. The tables also show the combination states $(n\nu_7+\nu_{10})^{\pm}$, $n = 1$ and 2, and $(\nu_{10}+\nu_{13})^{\pm}$. Interestingly, the 1+1 combinations largely mirror the structure of $\nu_{10}^{\pm}$, with each listed basis function now containing x_1 additionally. For the $(2\nu_7+\nu_{10})^{\pm}$, we note some minor contributions which point to the presence of anharmonic couplings between Q_7 and Q_{10}. The tunneling splittings for these combination states are lower than that for $\nu_{10}^{\pm}$. This is consistent with the pattern seen for the $n\nu_x^{\pm}$ states compared to $\nu_{gs}^{\pm}$.

Overall, the 4D eigenstates involving Q_7, Q_{13}, and Q_{27} are much easier to identify and assign via nodal patterns as well as comparisons to 3D results than those involving Q_5. Consequently, the tunneling splitting patterns for increasing excitations along these three modes as well as Q_{10} are very clearly seen.

TABLE S21. **Convergence of Q_1-Q_7-Q_{10}-Q_{29} states.** See the caption of Table S3 for notational details. The calculation with lower basis size was only done by changing the basis size for Q_7, as the convergence check for other coordinates were done with lower dimensional calculations.

M	Label	E_M		Δ		$\|\%\Delta_{err}\|$
		(18, 8, 17, 7)	(18, 6, 17, 7)	(18, 8, 17, 7)	(18, 6, 17, 7)	
1	ν_{gs}^+	1344.70	1344.82			
2	ν_{gs}^-	1410.39	1410.44	65.69	65.62	0.11
3	ν_{10}^+	1654.45	1654.48			
4	ν_{10}^-	1812.96	1813.00	158.51	158.52	0.006
5	ν_7^+	1923.18	1922.45			
6	ν_7^-	1980.21	1979.93	57.03	57.48	0.79
7	$2\nu_{10}^+$	2021.61	2021.50			
9	$2\nu_{10}^-$	2243.00	2243.01	221.39	221.51	0.05
8	$(\nu_7+\nu_{10})^+$	2235.97	2235.25			
10	$(\nu_7+\nu_{10})^-$	2384.00	2383.83	148.03	148.58	0.37
12	$2\nu_7^+$	2487.69	2489.15			
13	$2\nu_7^-$	2545.71	2546.36	58.02	57.21	1.40
11	$3\nu_{10}^+$	2425.69	2425.64			
15	$3\nu_{10}^-$	2684.58	2684.55	258.89	258.91	0.008
16	ν_1^+	2704.74	2705.02			
20	ν_1^-	2940.03	2940.17	235.29	235.15	0.06
17	$(\nu_{10}+2\nu_7)^+$	2801.92	2802.61			
21	$(\nu_{10}+2\nu_7)^-$	2950.89	2950.99	148.97	148.38	0.40

TABLE S22. **Four-dimensional eigenstates in Q_1-Q_{10}-Q_{13}-Q_{29} subspace,** their description,assignment, and tunneling splittings. The columns follow those of Table IV for Q_1-Q_{10} states in the manuscript. Contour plots for selected states are given in Fig. S11 below.

M	Label	E_M	E_M^{ex}	Δ	Description
1	ν_{gs}^+	1449.0	0.0		$+0.8626\ 1_{0^+}10_0 13_0 29_0$
2	ν_{gs}^-	1508.7	59.7	59.7	$+0.8919\ 1_{0^-}10_0 13_0 29_0$
3	ν_{10}^+	1754.6	305.6		$+0.6383\ 1_{0^+}10_1 13_0 29_0$ $+0.3079\ 1_{1^+}10_0 13_0 29_0$ $+0.2628\ 1_{1^+}10_2 13_0 29_0$ $-0.2503\ 1_{0^+}10_3 13_0 29_0$ $+0.2320\ 1_{0^+}10_2 13_0 29_0$
4	ν_{10}^-	1906.8	457.8	152.2	$+0.7729\ 1_{0^-}10_1 13_0 29_0$ $+0.2250\ 1_{1^-}10_0 13_0 29_0$ $+0.2245\ 1_{1^-}10_2 13_0 29_0$
5	$2\nu_{10}^+$	2116.4	667.4		$+0.4434\ 1_{0^+}10_2 13_0 29_0$ $-0.3147\ 1_{0^+}10_1 13_0 29_0$ $+0.2864\ 1_{1^+}10_1 13_0 29_0$ $-0.2797\ 1_{1^+}10_3 13_0 29_0$ $-0.2644\ 1_{0^+}10_0 13_0 29_0$ $-0.2473\ 1_{0^+}10_4 13_0 29_0$
8	$2\nu_{10}^-$	2332.5	883.5	216.1	$+0.6648\ 1_{0^-}10_2 13_0 29_0$ $-0.2604\ 1_{1^-}10_3 13_0 29_0$ $+0.2272\ 1_{1^-}10_1 13_0 29_0$
6	ν_{13}^+	2247.6	798.6		$+0.8408\ 1_{0^+}10_0 13_1 29_0$
7	ν_{13}^-	2297.6	848.6	50.0	$+0.8604\ 1_{0^-}10_0 13_1 29_0$
9	$3\nu_{10}^+$	2517.1	1068.1		$+0.3322\ 1_{0^+}10_3 13_0 29_0$ $+0.3179\ 1_{0^+}10_2 13_0 29_0$ $+0.2771\ 1_{0^+}10_1 13_0 29_0$ $+0.2722\ 1_{1^+}10_4 13_0 29_0$ $+0.2375\ 1_{0^+}10_5 13_0 29_0$ $+0.2250\ 1_{1^+}10_0 13_0 29_0$
12	$3\nu_{10}^-$	2768.2	1319.2	251.1	$+0.5702\ 1_{0^-}10_3 13_0 29_0$ $+0.2782\ 1_{1^-}10_4 13_0 29_0$ $+0.2387\ 1_{0^-}10_1 13_0 29_0$ $+0.2330\ 1_{0^-}10_5 13_0 29_0$
10	$(\nu_{10}+\nu_{13})^+$	2557.7	1108.7		$+0.6168\ 1_{0^+}10_1 13_1 29_0$ $+0.2865\ 1_{1^+}10_0 13_1 29_0$ $+0.2444\ 1_{0^+}10_2 13_1 29_0$ $-0.2430\ 1_{0^+}10_3 13_1 29_0$ $+0.2396\ 1_{1^+}10_2 13_1 29_0$
11	$(\nu_{10}+\nu_{13})^-$	2696.1	1247.1	138.4	$+0.7316\ 1_{0^-}10_1 13_1 29_0$
13	ν_1^+	2806.5	1357.5		$+0.5287\ 1_{1^+}10_0 13_0 29_0$ $+0.3812\ 1_{1^+}10_1 13_0 29_0$ $+0.3721\ 1_{0^+}10_0 13_0 29_1$ $-0.3290\ 1_{0^+}10_1 13_0 29_0$
16	ν_1^-	3035.4	1586.4	228.9	$+0.5192\ 1_{0^-}10_0 13_0 29_1$ $+0.4788\ 1_{1^-}10_0 13_0 29_0$ $-0.3110\ 1_{0^-}10_1 13_0 29_0$ $+0.2745\ 1_{0^-}10_0 13_0 29_0$
17	$2\nu_{13}^+$	3038.1	1589.1		$+0.8103\ 1_{0^+}10_0 13_2 29_0$ $+0.2357\ 1_{0^+}10_1 13_2 29_0$
18	$2\nu_{13}^-$	3086.5	1637.5	48.4	$+0.8171\ 1_{0^-}10_0 13_2 29_0$

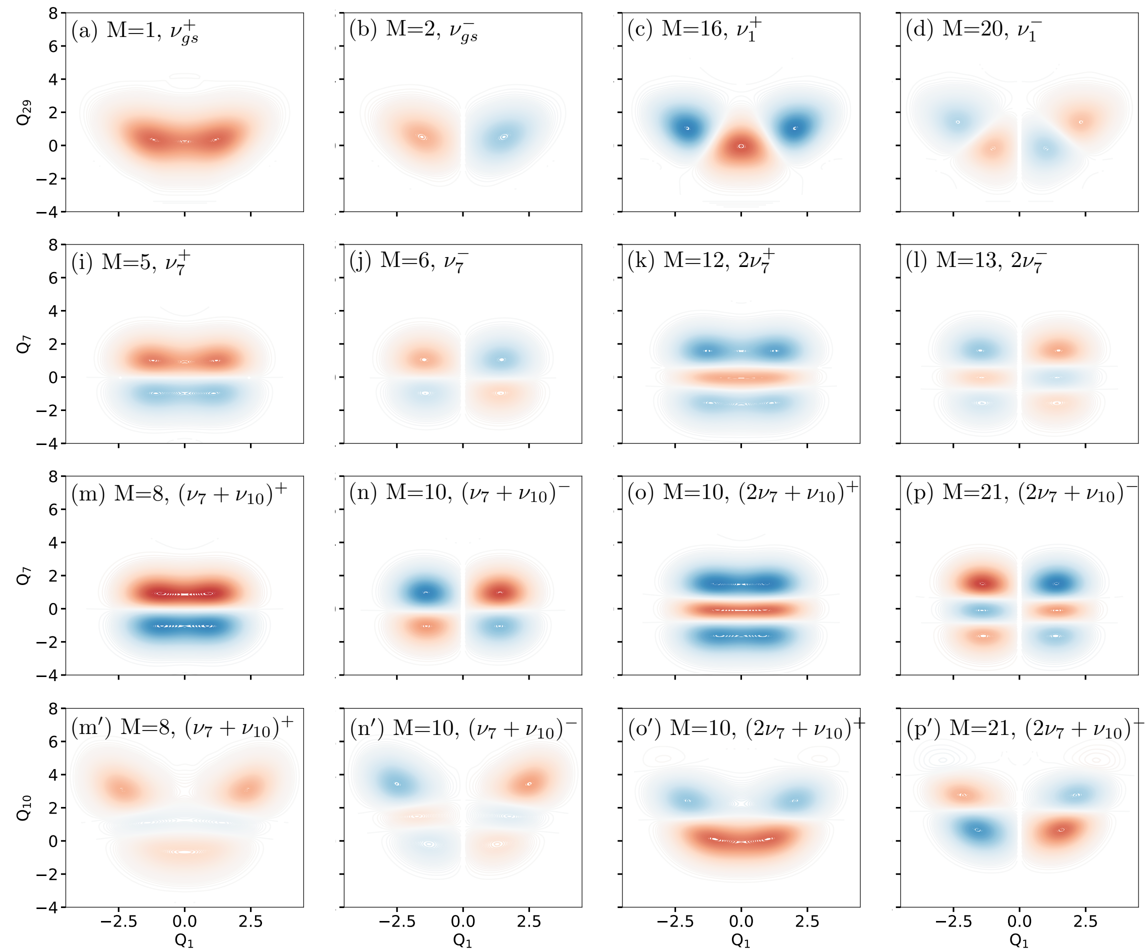

FIG. S10. **Plots of Q_1-Q_7-Q_{10}-Q_{29} 4D eigenstates.** The descriptions of these states are given in S20 above. The labelling is consistent with the nodal pattern in each plot.

TABLE S23. **Convergence of Q_1-Q_{10}-Q_{13}-Q_{29} states.** See the caption of Table S3 for notational details. The calculation with lower basis size was only done by changing the basis size for Q_{13}, as the convergence check for other coordinates were done with lower dimensional calculations.

M	Label	E_M		Δ		$\lvert \%\Delta_{err} \rvert$
		(18, 17, 7, 7)	(18, 17, 6, 7)	(18, 17, 7, 7)	(18, 17, 6, 7)	
1	ν_{gs}^+	1448.97	1449.15			
2	ν_{gs}^-	1508.71	1508.79	59.74	59.64	0.17
3	ν_{10}^+	1754.60	1754.84			
4	ν_{10}^-	1906.82	1906.94	152.22	152.10	0.08
5	$2\nu_{10}^+$	2116.39	2116.47			
8	$2\nu_{10}^-$	2332.52	2332.48	216.13	216.01	0.06
6	ν_{13}^+	2247.60	2247.29			
7	ν_{13}^-	2297.60	2297.40	50.0	50.11	0.22
9	$3\nu_{10}^+$	2517.08	2517.04			
12	$3\nu_{10}^-$	2768.24	2767.90	251.16	250.86	0.12
10	$(\nu_{10}+\nu_{13})^+$	2557.65	2557.91			
11	$(\nu_{10}+\nu_{13})^-$	2696.11	2696.34	138.46	138.43	0.02
13	ν_1^+	2806.54	2807.03			
16	ν_1^-	3035.42	3035.79	228.88	228.76	0.05
17	$2\nu_{13}^+$	3038.10	3039.54			
18	$2\nu_{13}^-$	3086.47	3087.38	48.37	47.84	1.10

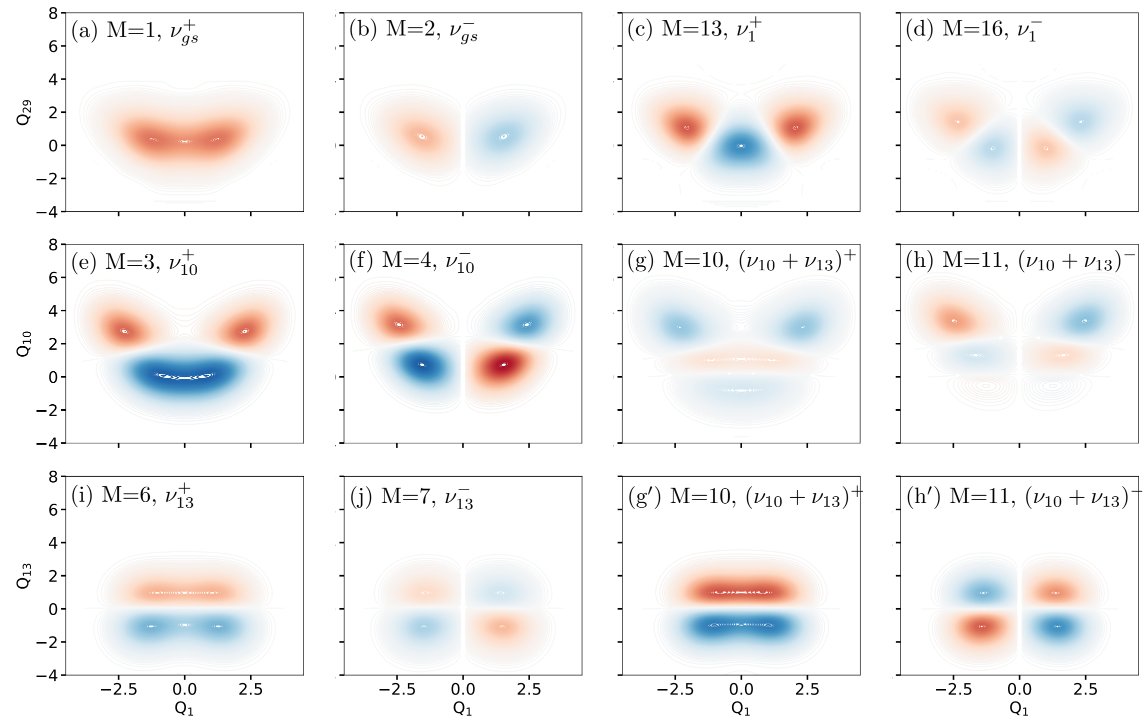

FIG. S11. **Plots of Q_1-Q_{10}-Q_{13}-Q_{29} 4D eigenstates.** The descriptions of these states are given in S22 above. The labelling is consistent with the nodal pattern in each plot.

TABLE S24. **Four dimensional eigenstates in Q_1-Q_{10}-Q_{27}-Q_{29} subspace,their description, assignment, and tunneling splittings.** The columns follow those of Table IV for Q_1-Q_{10} states in the manuscript. Contour plots for selected states are given in Fig. S12 below.

M	Label	E_M	E_M^{ex}	Δ	Description
1	v_{gs}^+	1839.7	0.0		$+0.8600\ 1_{0^+}10_0 27_0 29_0$ $+0.2318\ 1_{0^+}10_1 27_0 29_0$
2	v_{gs}^-	1902.0	62.3	62.3	$+0.8948\ 1_{0^-}10_0 27_0 29_0$
3	v_{10}^+	2150.1	310.3		$+0.6330\ 1_{0^+}10_1 27_0 29_0$ $+0.3123\ 1_{1^+}10_0 27_0 29_0$ $+0.2618\ 1_{1^+}10_2 27_0 29_0$ $-0.2539\ 1_{0^+}10_3 27_0 29_0$ $+0.2413\ 1_{0^+}10_2 27_0 29_0$
4	v_{10}^-	2306.3	466.6	156.3	$+0.7852\ 1_{0^-}10_1 27_0 29_0$ $+0.2333\ 1_{1^-}10_0 27_0 29_0$
5	$2v_{10}^+$	2520.8	681.1		$+0.4396\ 1_{0^+}10_2 27_0 29_0$ $-0.3498\ 1_{0^+}10_1 27_0 29_0$ $+0.2922\ 1_{1^+}10_1 27_0 29_0$ $-0.2802\ 1_{1^+}10_3 27_0 29_0$ $-0.2531\ 1_{0^+}10_0 27_0 29_0$ $-0.2521\ 1_{0^+}10_4 27_0 29_0$
6	$2v_{10}^-$	2740.9	901.2	220.1	$+0.6894\ 1_{0^-}10_2 27_0 29_0$ $-0.2634\ 1_{1^-}10_3 27_0 29_0$ $+0.2420\ 1_{1^-}10_1 27_0 29_0$
7	$3v_{10}^+$	2931.1	1091.4		$+0.3490\ 1_{0^+}10_2 27_0 29_0$ $+0.3357\ 1_{0^+}10_3 27_0 29_0$ $+0.2754\ 1_{1^+}10_4 27_0 29_0$ $+0.2475\ 1_{1^+}10_0 27_0 29_0$ $+0.2465\ 1_{0^+}10_5 27_0 29_0$ $+0.2448\ 1_{0^+}10_1 27_0 29_0$
9	$3v_{10}^-$	3187.4	1347.7	256.3	$+0.6037\ 1_{0^-}10_3 27_0 29_0$ $+0.2854\ 1_{1^-}10_4 27_0 29_0$ $+0.2442\ 1_{0^-}10_5 27_0 29_0$ $+0.2391\ 1_{0^-}10_1 27_0 29_0$
8	v_1^+	3157.6	1317.9		$+0.4965\ 1_{1^+}10_0 27_0 29_0$ $+0.3515\ 1_{1^+}10_1 27_0 29_0$ $-0.3380\ 1_{0^+}10_1 27_0 29_0$ $+0.3364\ 1_{0^+}10_0 27_0 29_1$ $-0.2421\ 1_{0^+}10_0 27_1 29_0$
10	v_1^-	3355.7	1516.0	198.1	$+0.4691\ 1_{0^-}10_0 27_1 29_0$ $-0.3981\ 1_{1^-}10_0 27_0 29_0$ $-0.3785\ 1_{0^-}10_0 27_0 29_1$ $+0.3071\ 1_{0^-}10_1 27_0 29_0$ $-0.2823\ 1_{0^-}10_0 27_0 29_0$
12	v_{27}^+	3471.0	1631.3		$+0.7952\ 1_{0^+}10_0 27_1 29_0$
13	v_{27}^-	3559.0	1719.3	88.0	$+0.7447\ 1_{0^-}10_0 27_1 29_0$ $+0.3590\ 1_{0^-}10_0 27_0 29_1$ $+0.2634\ 1_{1^-}10_0 27_0 29_0$

TABLE S25. **Convergence of Q_1-Q_{10}-Q_{27}-Q_{29} states.** See the caption of Table S3 for notational details. The calculation with lower basis size was only done by changing the basis size for Q_{27}, as the convergence check for other coordinates were done with lower dimensional calculations.

M	Label	E_M		Δ		$\lvert\%\Delta_{err}\rvert$
		(18, 17, 6, 7)	(18, 17, 5, 7)	(18, 17, 6, 7)	(18, 17, 5, 7)	
1	ν_{gs}^{+}	1839.67	1839.31			
2	ν_{gs}^{-}	1901.95	1901.73	62.28	62.42	0.22
3	ν_{10}^{+}	2150.11	2150.06			
4	ν_{10}^{-}	2306.33	2306.02	156.22	155.96	0.17
5	$2\nu_{10}^{+}$	2520.81	2520.96			
6	$2\nu_{10}^{-}$	2740.91	2740.65	220.10	219.69	0.19
7	$3\nu_{10}^{+}$	2931.10	2930.81			
9	$3\nu_{10}^{-}$	3187.38	3187.29	256.28	256.48	0.08
8	ν_{1}^{+}	3157.64	3156.67			
10	ν_{1}^{-}	3355.72	3355.61	198.08	198.94	0.43
12	ν_{27}^{+}	3471.00	3472.74			
13	ν_{27}^{-}	3558.96	3559.54	87.96	86.80	1.32

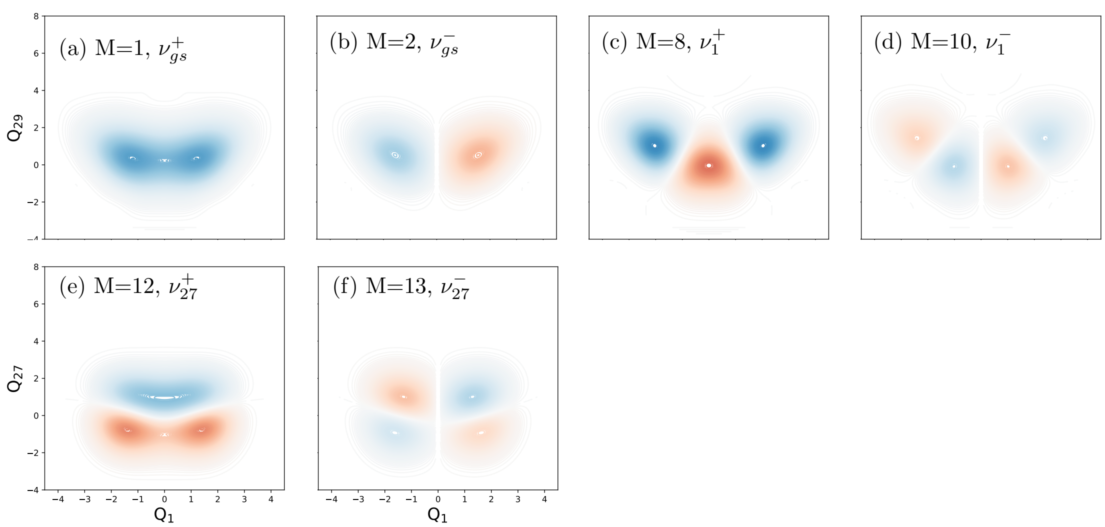

FIG. S12. **Plots of Q_1-Q_{10}-Q_{27}-Q_{29} 4D eigenstates.** The descriptions of these states are given in S24 above. The labelling is consistent with the nodal pattern in each plot.

IV. Eigenstates partially relaxed potentials

The introductory text in Sec. 3 of the manuscript as well as Sec. 3.3 describe how partially relaxed potentials are obtained for n-mode spaces, denoted S_{nr}. We note that additional potential corrections as decribed in Appendix B of the manuscript are used here. These are subsequently used to obtain nD eigenstates for these spaces. Those for $S_{3r} = (Q_1, Q_{10}, Q_{29})$ are described in the manuscript in Sec. 3.3. Presently, we describe the results for $S_{1r} = (Q_1)$ and $S_{2r} = (Q_1, Q_{10})$.

A. Q_1 eigenstates

Fig. S13 shows the relaxed potential along Q_1, where all other coordinates are relaxed. Note that this includes the potential corrections described in Appendix B, especially correction 2 there. Absent this, for region $|Q_1| \approx 6$, the DGEVB potential shows an unphysical maximum. The correction adds a repulsive function that is mainly effective for $|Q_1| \gtrsim 5$ and begins with a soft increase followed by rapid increase.

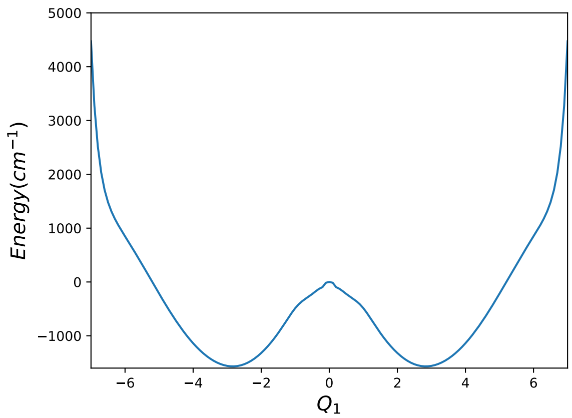

FIG. S13. **Plot of the relaxed potential as a function of Q_1.** All other normal modes are relaxed. See Appendix B of the manuscript regarding the additional diabatic corrections used towards the relaxed potentials.

The calculated 1D eigenstates are given in Table S26. These are obtained directly in a sinc-DVR basis of size 71. The ground state splitting is found to be 11.1 cm^{-1}. With increasing excitation in Q_1, the tunneling splitting expectly increases strongly.

TABLE S26. **Eigenstates for $S_{1r} = (Q_1)$ with a relaxed potential.** A sinc-DVR basis of size 71 was used in the range [-7.0, 7.0] to obtain the eigenstates.

M	Label	E_M	E_M^{ex}	Δ
1	ν_{gs}^+	-1132.1	0.0	
2	ν_{gs}^-	-1121.0	11.1	11.1
3	ν_1^+	-359.6	772.5	
4	ν_1^-	-239.6	892.5	120.0
5	$2\nu_1^+$	292.5	1424.6	
6	$2\nu_1^-$	641.2	1773.3	348.7

B. Q_1-Q_{10} 2D eigenstates

With the corrected potential (Appendix B of the manuscript), Fig. S14 shows the 2D relaxed potential in (Q_1, Q_{10}) space. The potential is qualitatively similar to the unrelaxed one, albeit with the full barrier height recovered and spanning a larger coordinate range.

Selected eigenstates computed with a (50, 50) PODVR basis with this potential are enumerated in Table S27 and plotted in Fig. S15. The tunneling splitting of the ground state pair ($\nu_{gs}^{\pm}$) is interestingly lowered to 7.8 cm^{-1} from 11.1

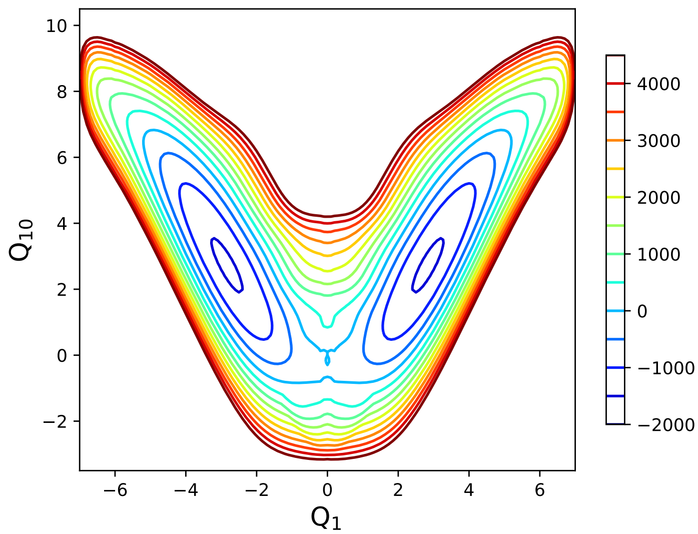

FIG. S14. **Plot of the partial relaxed potential in the $S_{2r} = (Q_1, Q_{10})$ mode space.** Contours have a 500 cm^{-1} spacing

cm^{-1} in the ground state. The next pair several pairs of excited states are identified as $n\nu_{10}^{\pm}$. For the two excitations, the dominant expansion coefficients also support the assignment. For higher excitations, the coefficients are more mixed but the wavefunction plots clearly indicate the assignment. The tunneling splittings expectedly increase with excitation. The state pair 12 and 14 are assigned to $\nu_1^{\pm}$. The latter is clearly so from both the dominant expansion coefficient as well as the wavefunction plot. However, state 12 is a mixture of a Q_{10} excitation (likely with 5 quanta) and a Q_1 excitation as seen from the wavefunction pattern. State 11 (not shown) appears to be the counterpart of this admixture; a comparison of the nodal patterns of states 11 and 12 suggest that the latter has a dominant Q_1 excitation contribution.

TABLE S27. **2D eigenstates in the (Q_1, Q_{10}) space with a partially relaxed potential.**

M	Label	E_M	E_M^{ex}	Δ	Description
1	ν_{gs}^+	−471.8	0.0		$+0.9324\ 1_{0^+}10_0\ -0.2687\ 1_{1^+}10_1$
2	ν_{gs}^-	−463.9	7.8	7.8	$+0.9427\ 1_{0^-}10_0\ -0.2565\ 1_{1^-}10_1$
3	ν_{10}^+	−166.8	304.9		$+0.7457\ 1_{0^+}10_1\ -0.3734\ 1_{1^+}10_2\ -0.3177\ 1_{1^+}10_0$ $-0.2247\ 1_{0^+}10_3$
4	ν_{10}^-	−130.0	341.8	36.9	$+0.7935\ 1_{0^-}10_1\ -0.3548\ 1_{1^-}10_2\ -0.3216\ 1_{1^-}10_0$
5	$2\nu_{10}^+$	124.5	596.3		$+0.5272\ 1_{0^+}10_2\ +0.3870\ 1_{1^+}10_3\ -0.2839\ 1_{0^+}10_0$ $-0.2797\ 1_{1^+}10_1\ +0.2579\ 1_{2^+}10_2\ -0.2304\ 1_{2^+}10_4$ $-0.2272\ 1_{0^+}10_4$
6	$2\nu_{10}^-$	212.8	684.6	88.3	$+0.6289\ 1_{0^-}10_2\ +0.3928\ 1_{1^-}10_3\ -0.3127\ 1_{1^-}10_1$ $-0.2704\ 1_{0^-}10_0\ -0.2420\ 1_{0^-}10_4\ +0.2271\ 1_{2^-}10_2$
7	$3\nu_{10}^+$	427.2	898.9		$+0.4061\ 1_{0^+}10_1\ -0.3394\ 1_{1^+}10_4\ +0.3342\ 1_{0^+}10_3$ $+0.2730\ 1_{2^+}10_3\ +0.2623\ 1_{2^+}10_5\ -0.2444\ 1_{0^+}10_2$
8	$3\nu_{10}^-$	569.2	1041.0	142.3	$+0.4674\ 1_{0^-}10_3\ -0.3902\ 1_{1^-}10_4\ +0.3742\ 1_{0^-}10_1$ $+0.2460\ 1_{2^-}10_3\ +0.2429\ 1_{0^-}10_5\ +0.2298\ 1_{1^-}10_2$ $+0.2242\ 1_{2^-}10_5$
9	$4\nu_{10}^+$	755.0	1226.8		$+0.4433\ 1_{0^+}10_2\ -0.2791\ 1_{1^+}10_5\ -0.2645\ 1_{2^+}10_6$ $-0.2482\ 1_{1^+}10_1\ +0.2403\ 1_{2^+}10_4$
10	$4\nu_{10}^-$	932.6	1404.4	177.6	$+0.3996\ 1_{0^-}10_2\ -0.3586\ 1_{1^-}10_5\ +0.3242\ 1_{0^-}10_4$ $-0.2405\ 1_{2^-}10_6\ +0.2290\ 1_{2^-}10_4\ -0.2262\ 1_{0^-}10_6$
12	ν_1^+	1134.6	1606.4		$+0.4990\ 1_{1^+}10_0\ -0.4604\ 1_{0^+}10_3\ -0.2410\ 1_{2^+}10_1$
14	ν_1^-	1344.5	1816.2	209.8	$+0.8463\ 1_{1^-}10_0\ +0.3712\ 1_{0^-}10_1\ -0.2889\ 1_{2^-}10_1$

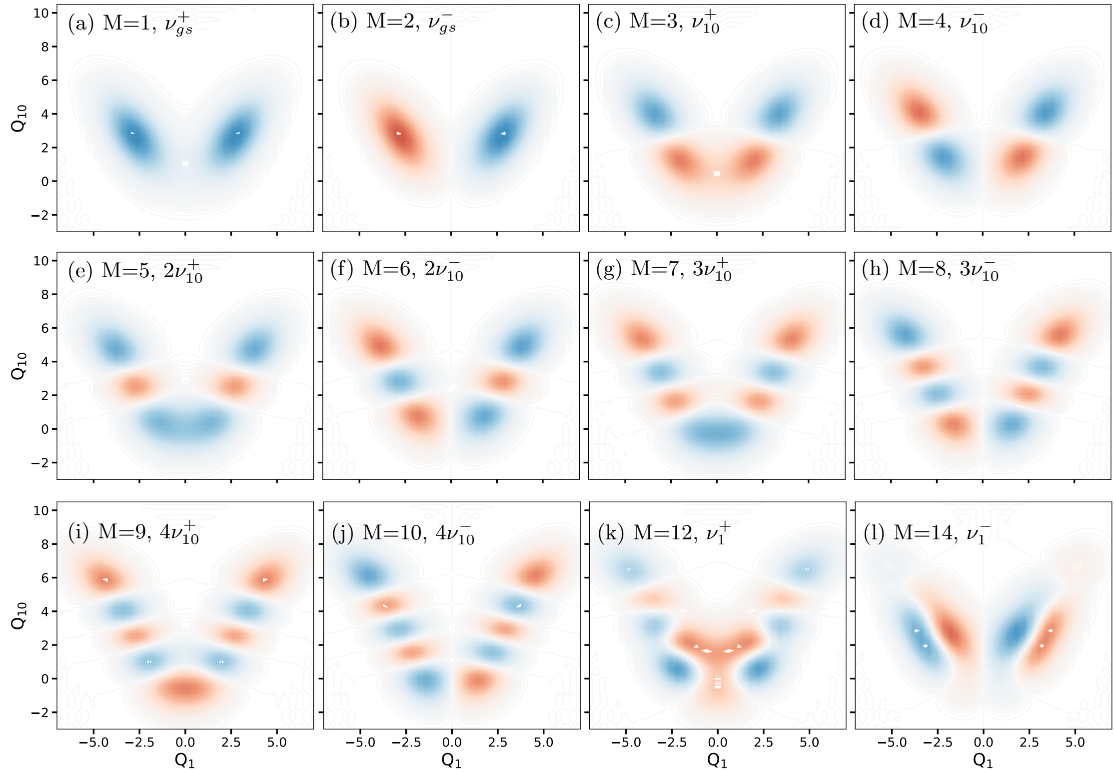

FIG. S15. **Plots of selected $S_{2r} = (Q_1, Q_{10})$ eigenstates.** Their assignments and descriptions are given in Table S27.

C. Q_1-Q_{10}-Q_{29} 3D eigenstates - convergence

Section 3.3 of the manuscript describes the 3D Q_1-Q_{10}-Q_{29} eigenstates with a partially relaxed PES. The calculations were carried out there with a (54, 32, 18) PODVR basis in the three modes. Here, we provide convegence plots. Fig. S16(a) shows the convergence as a function of number of PODVR functions in Q_1; a substantial number of functions was required before they sufficiently spanned the coordinate space. Fig. S16(b) shows the convergence with respect to the Q_{10} and Q_{29}, which is very good with fewer points that for Q_1.

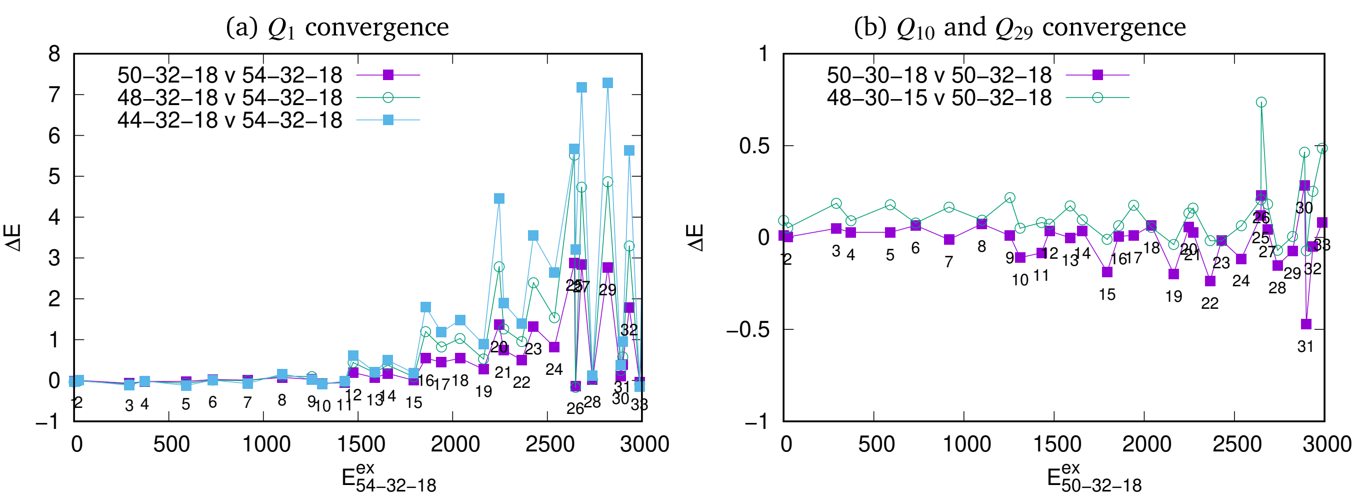

FIG. S16. **Convergence of $S_{3r} = (Q_1, Q_{10}, Q_{29})$ eigenstates.** Plotted are the differences in the eigenstates computed with various PODVR bases as a function of the state excitation energy. Both axes are in cm^{-1} units.

References

[1] H. Guo and B. Jiang, Acc. Chem. Res. **47**, 3679 (2014).
[2] P. Houston, R. Conte, C. Qu, and J. M. Bowman, J. Chem. Phys. **153**, 024107 (2020).
[3] Y. Wang and J. M. Bowman, J. Chem. Phys. **139**, 154303 (2013).
[4] V. Benderskii, V. Goldanskii, and D. Makarov, Chem. Phys. **154**, 407 (1991).
[5] V. Benderskii, V. Goldanskii, and D. Makarov, Chem. Phys. **159**, 29 (1992).
[6] V. Benderskii, D. Makarov, and P. Grinevich, Chem. Phys. **170**, 275 (1993).
[7] S. Takada and H. Nakamura, J. Chem. Phys. **100**, 98 (1994).
[8] S. Takada and H. Nakamura, J. Chem. Phys. **102**, 3977 (1995).
[9] J. L. Bao and D. G. Truhlar, Chem. Soc. Rev. **46**, 7548 (2017).
[10] M. T. Cvitaš and S. C. Althorpe, J. Chem. Theory Comput. **12**, 787 (2016).
[11] H. Nakamura and G. Mil'nikov, *Quantum mechanical tunneling in chemical physics* (CRC Press, 2013).
[12] K. Giese, M. Petković, H. Naundorf, and O. Kühn, Phys. Rep. **430**, 211 (2006).
[13] C. R. Harris, K. J. Millman, S. J. van der Walt, R. Gommers, P. Virtanen, D. Cournapeau, E. Wieser, J. Taylor, S. Berg, N. J. Smith, R. Kern, M. Picus, S. Hoyer, M. H. van Kerkwijk, M. Brett, A. Haldane, J. F. del Río, M. Wiebe, P. Peterson, P. Gérard-Marchant, K. Sheppard, T. Reddy, W. Weckesser, H. Abbasi, C. Gohlke, and T. E. Oliphant, Nature **585**, 357 (2020).